การสังเคราะห์ฟิชเชอร์-ทรอปช์บนตัวเร่งปฏิกิริยาโคบอลต์รองรับด้วยซิลิกาทรงกลมแบบกลวง

นางสาวธัชพรรณ อัจจิมารังษี

วิทยานิพนธ์นี้เป็นส่วนหนึ่งของการศึกษาตามหลักสูตรปริญญาวิทยาศาสตรมหาบัณฑิต
สาขาวิชาปิโตรเคมีและวิทยาศาสตร์พอลิเมอร์
คณะวิทยาศาสตร์ จุฬาลงกรณ์มหาวิทยาลัย
ปีการศึกษา 2559

FISCHER-TROPSCH SYNTHESIS OVER COBALT SUPPORTED ON SILICA HOLLOW SPHERE CATALYST

Miss Thachapan Atchimarungsri

A Thesis Submitted in Partial Fulfillment of the Requirements
for the Degree of Master of Science Program in Petrochemistry and Polymer Science
Faculty of Science
Chulalongkorn University
Academic Year 2016

Thesis Title	FISCHER- TROPSCH SYNTHESIS OVER COBALT SUPPORTED ON SILICA HOLLOW SPHERE CATALYST
By	Miss Thachapan Atchimarungsri
Field of Study	Petrochemistry and Polymer Science
Thesis Advisor	Associate Professor Prasert Reubroycharoen, Ph.D.

Accepted by the Faculty of Science, Chulalongkorn University in Partial Fulfillment of the Requirements for the Master's Degree

.....Dean of the Faculty of Science
(Associate Professor Polkit Sangvanich, Ph.D.)

THESIS COMMITTEE

.....Chairman
(Assistant Professor Sirithan Jiemsirilers, Ph.D.)

.....Thesis Advisor
(Associate Professor Prasert Reubroycharoen, Ph.D.)

.....Examiner
(Associate Professor Napida Hinchiranan, Ph.D.)

.....External Examiner
(Assistant Professor Chanatip Samart, Ph.D.)

ธัชพรรณ อัจจิมารังษี : การสังเคราะห์ฟิชเชอร์-ทรอปช์บนตัวเร่งปฏิกิริยาโคบอลต์รองรับด้วยซิลิกาทรงกลมแบบกลวง (FISCHER-TROPSCH SYNTHESIS OVER COBALT SUPPORTED ON SILICA HOLLOW SPHERE CATALYST) อ.ที่ปรึกษาวิทยานิพนธ์หลัก: รศ. ดร. ประเสริฐ เรียบร้อยเจริญ, 71 หน้า.

งานวิจัยนี้ศึกษาตัวเร่งปฏิกิริยาโคบอลต์ที่ใช้ซิลิกาทรงกลมแบบกลวงเป็นตัวรองรับในการสังเคราะห์ฟิสเชอร์-ทรอปช์ เนื่องจากปกติโดยทั่วไปปัญหาหลักของการสังเคราะห์ฟิสเชอร์-ทรอปช์บนตัวเร่งปฏิกิริยาโคบอลต์บนตัวรองรับซิลิกาทางการค้าทั่วไปให้ผลิตภัณฑ์ของสารประกอบไฮโดรคาร์บอนที่มักมีช่วงกว้าง งานวิจัยนี้จึงมีความสนใจเพื่อแก้ปัญหาดังกล่าว เนื่องจากตัวรองรับซิลิกาทรงกลมแบบกลวงมีผนังของช่องว่างตรงกลางในตัวเร่งปฏิกิริยาที่ช่วยให้เกิดการยับยั้งการเจริญเติบโตของสายโซ่ของสารประกอบไฮโดรคาร์บอน โดยนำมาผ่านวิธีการโหลดโลหะโคบอลต์บนตัวรองรับซิลิกาด้วยวิธีการเอิบชุ่ม (wetness impregnation method) เพื่อใช้ในการเร่งปฏิกิริยาการสังเคราะห์ฟิสเชอร์-ทรอปช์ โดยเตรียมตัวรองรับซิลิกาแบบทรงกลมกลวงด้วยวิธีอิมัลชัน (Emulsion) ของน้ำในชั้นน้ำมัน และในชั้นน้ำ (W/O/W) ซึ่งใช้โซเดียมซิลิเกต (Sodium silicate) เป็นแหล่งของซิลิกา และใช้แอมโมเนียมไฮโดรเจนคาร์บอเนต (NH_4HCO_3) สำหรับรูพรุนชนิดเมโซพอรัสของตัวรองรับซิลิกาแบบทรงกลมกลวง และได้ลักษณะของตัวรองรับชนิดซิลิกาแบบทรงกลมกลวงที่เหมาะสมคือ มีพื้นที่ผิวจำเพาะมากกว่า 500 ตารางเมตรต่อกรัมของตัวรองรับ และมีพื้นที่ผิวของรูพรุนขนาดไมโครเมตรน้อยกว่า 20 ตารางเมตรต่อกรัมของตัวเร่งปฏิกิริยา พบว่าให้ค่าร้อยละการเปลี่ยนแปลงคาร์บอนมอนนอกไซด์ที่สูงมากกว่าร้อยละ 90 เปอร์เซ็นต์ โดยให้ค่าการเลือกเกิดสารประกอบไฮโดร์คาร์บอนมากกว่าหรือเท่ากับ 12 ที่ต่ำ และให้ค่าการกระจายของผลิตภัณฑ์สารประกอบไฮโดรคาร์บอนที่ช่วงแคบกว่าตัวเร่งปฏิกิริยาทางการค้า นอกจากนี้ได้ศึกษาการเคลือบซีโอไลต์ชนิด ZSM-5 บนตัวเร่งปฏิกิยาโคบอลต์ที่รองรับด้วยตัวรองรับซิลิกาแบบทรงกลมกลวงด้วย 2 วิธี ได้แก่ วิธีไฮโดรเทอร์มอล (Hydrothermal synthesis) และวิธีการใช้ไอน้ำช่วยในการตกผลึก (Steam-assisted crystallization; SAC) พบว่าให้ผลิตภัณฑ์ในช่วงที่แคบเพิ่มมากขึ้น และเกิดผลิตภัณฑ์ของไอโซพาราฟิน และโอเลฟินเพิ่มขึ้นเนื่องจากซีโอไลต์มีความเป็นกรดช่วยทำให้เกิดปฏิกิริยาไอโซเมอไรเซชันเพิ่มขึ้น แต่อย่างไรก็ตามวิธีการปรับปรุงตัวเร่งปฏิกิริยาด้วยการเคลือบซีโอไลต์บนตัวเร่งปฏิกิริยา พบว่ายังมีปัญหาต่างๆ เช่น การสลายตัวของตัวรองรับซิลิกา การหลุดออกของโลหะโคบอลต์บนตัวรองรับซิกา และการที่ซีโอไลต์ไม่เคลือบบนตัวเร่งปฏิกิริยาทำให้ค่าร้อยละของการเปลี่ยนแปลงคาร์บอนมอนนอกไซด์ที่ต่ำ

สาขาวิชา ปิโตรเคมีและวิทยาศาสตร์พอลิเมอร์ ลายมือชื่อนิสิต .....

ปีการศึกษา 2559 ลายมือชื่อ อ.ที่ปรึกษาหลัก .....

5772013023 : MAJOR PETROCHEMISTRY AND POLYMER SCIENCE
KEYWORDS: FISCHER-TROPSCH SYNTHESIS / SILICA HOLLOW SPHERE / COBALT

THACHAPAN ATCHIMARUNGSRI: FISCHER-TROPSCH SYNTHESIS OVER COBALT SUPPORTED ON SILICA HOLLOW SPHERE CATALYST. ADVISOR: ASSOC. PROF. PRASERT REUBROYCHAROEN, Ph.D., 71 pp.

A propose of this work studied the silica hollow sphere (SHS) for a proper characteristic of support in the Fischer-Tropsch synthesis (FTS) because the normally main problem of FTS reaction was being produced the broader hydrocarbon products on a commercial catalyst. Nevertheless, the hollow sphere shape of SHS catalyst had a wall of the core catalyst for steric restriction of hydrocarbon propagation. The cobalt metals were loaded on the SHS by wetness impregnation method and used in the FTS. The SHS was synthesized through emulsion process with water/oil/water (W/O/W) that used the sodium silicate for silica source and NH_4HCO_3 for the mesopore generating in the SHS support. The proper SHS catalyst in FTS showed higher specific surface area more than 500 m^2/g and less micropore, causing diffusion elimination and mass transfer inside the pore, which resulted in the enhanced CO conversion more than 90 percent, lower C_{12+}, and the narrower hydrocarbon selectivity. Moreover, the study of the coated zeolite that was ZSM-5 type on the SHS catalyst was two methods, which were hydrothermal synthesis and steam-assisted crystallization (SAC) process. The results of both methods represented the increase of narrower hydrocarbon products, isoparaffins and olefins selectivity due to acid sites of the zeolite. However, these methods as the improved cobalt based over SHS catalyst had some problems such as the decomposing of the silica, removing of cobalt metals on the SHS support and uncovering of some zeolite over the SHS catalysts.

Field of Study: Petrochemistry and Polymer Science Student's Signature .....
Advisor's Signature .....

Academic Year: 2016

ACKNOWLEDGEMENTS

I would like to express my sincere thankfulness to my thesis advisor, Assoc. Prof. Dr. Prasert Reubroychareon for his invaluable assistance and still encouragement from the beginning until this time. I am very grateful to him for his teaching and advice throughout the course of this research which is not only research methodologies but also other life methodologies. Moreover, I am very grateful and I would like to thanks for the teachers at university of Toyama: Prof. Noritatsu Tsubaki and Prof. Yoshiharu Yoneyama who give opportunity and experience to me about study this research work, financially supported my research, and all their help and suggestions. I also would like to acknowledge Asst. Prof. Dr. Sirithan Jiemsirilers , Assoc. Prof. Dr. Napida Hinchiranan, and Asst. Prof. Dr. Chanathip Samart for serving as chairman and members of thesis committee, respectively and for their worthy criticisms and advices.

I would like to acknowledge the financial supported by Japan Science and Technology Agency (JST).

Many thanks are going to everyone in laboratory of Assoc. Prof. Dr. Prasert and Prof. Tsubaki for all help, suggestions, and teaching to use laboratory equipments. My research would not have been successful, if there are no their supports.

I also would like to thanks my parents for their love, sympathy and great support to me all the time. Additionally, thank you to my friends for friendship, cheerfulness and always being beside me.

CONTENTS

Page

THAI ABSTRACT iv

ENGLISH ABSTRACT v

ACKNOWLEDGEMENTS vi

CONTENTS vii

LIST OF FIGURES xi

LIST OF TABLES xiii

INTRODUCTION 1

1.1 Statement of problem 1

1.2 Studies of the thesis 3

1.3 Objectives 3

CHAPTER II 4

THEORY AND LITERATURE REVIEWS 4

2.1 Overview of the Fischer-Tropsch synthesis 4

2.2 Effect factors of activity and selectivity for the FTS 7

2.2.1 Active sites 7

2.2.1.1 Types of active sites 7

2.2.1.2 Cobalt catalyst particle sizes 7

2.2.1.3 Cobalt catalyst synthesis 8

2.2.2 Texture of supports 9

2.2.2.1 Types of catalyst supports 9

2.2.2.2 Pore size of catalyst support 10

2.2.2.3 Hybrid catalyst 11

Page

2.2.2.4 Mesoporous materials 12
2.2.3 Reaction conditions; Temperature, Gas Hourly Space Velocity, Syngas ratio and Total pressure 13
2.2.3.1 Temperature 13
2.2.3.2 Syngas ratio and Total pressure 14
2.2.3.3 Gas Hourly Space Velocity 14
2.2.4 Reactors 15
2.2.4.1 Slurry-phase reactor 15
2.2.4.2 Fixed-bed reactor 15
2.2.5 Other deactivation parameters 17
2.2.5.1 Alkali and alkaline earth metals 17
2.2.5.2 Sintering of cobalt crystallites 18
2.2.5.3 Re-oxidation 18
2.3 Literature reviews 18
CHAPTER III 21
EXPERIMENTAL 21
3.1 Materials and reagents 21
3.2 Catalyst preparation 21
3.2.1 Silica hollow sphere (SHS) preparation 21
3.2.2 Preparation of supported cobalt catalysts 22
3.2.3 Preparation of zeolite membrane coating on SHS 22
3.2.3.1 Hydrothermal method 22
3.2.3.2 Steam-assisted crystallization (SAC) process 23

Page

3.4 Catalyst characterization 23
3.4.1 N_2 physisorption 23
3.4.2 X-ray diffraction (XRD) 24
3.4.3 Scanning electron microscopy and energy dispersive spectroscopy (SEM-EDS) 24
3.4.5 Transmission electron microscopy (TEM) 24
3.4.6 H_2-Temperature-programmed reduction (H_2-TPR) 24
3.5 FTS reaction performance 24
CHAPTER IV 26
RESULTS AND DISCUSSION 26
4.1 Comparisons between Co based commercial silica and SHSs. 26
4.1.1 Structural and textural of catalysts 26
4.1.2 FTS performance of the SHS catalysts 36
4.1.3 Study of both with and without sonication during catalyst preparation. 38
4.1.3.1 Structural and textural of catalysts. 38
4.1.3.2 FTS performance of the catalysts 40
4.2 The improved catalyst with zeolite 42
4.2.1 Structural and textural of catalysts 42
4.2.2 FTS performance of the SHS catalysts 46
CHAPTER V 49
CONCLUSION AND RECOMMENDATION 49
5.1 Conclusion 49
5.1.1 Preparation of the cobalt based over silica hollow sphere catalyst 49

Page

5.1.2 Study of the catalytic activity of the cobalt based over silica hollow sphere catalyst in FTS 49

5.1.3 Study of the catalytic activity of the modified cobalt based over silica hollow sphere catalyst with ZSM-5 in FTS 50

5.2 Recommendation 50

REFERENCES 51

APENDIX 57

VITA 71

LIST OF FIGURES

Figure 1 Schematic of the propagation to long-chain length 5

Figure 2 Chain growth pathways and possible secondary reactions of olefins in the FTS 5

Figure 3 Influence of cobalt particle size on (a) the TOF at 35 bar and 210 ° C (b) the methane selectivity at 1 bar and 210 ° C, and (c) the C_{5+} selectivity at 35 bar with data markers in black at 210 ° C and in gray at 250 ° C 8

Figure 4 Relation between pore diameters, sizes of supported Co_3O_4 particles, and FTS reaction rates over cobalt catalysts supported by mesoporous silicas 10

Figure 5 Schematic image of the capsule catalyst role in the FTS reaction .. 12

Figure 6 Synthesis schematic route of iron-based micro-capsule catalyst in SAC process 12

Figure 7 Effect of temperature on C_{5+}selectivity for a Co/Ru/alumina catalyst operated in a slurry reactor 13

Figure 8 Schematic of FTS reactor type used commercially between slurry-phase reactor (left) and multitubular fixed-bed reactor (right) 16

Figure 9 Schematic of FTS system 25

Figure 10 Nitrogen sorption isotherms of samples (a) and pore size distribution of samples in mesoporous region (b) 26

Figure 11 XRD patterns of the catalysts 29

Figure 12 SEM images of samples: (a) Co/Q-10, (b) Co/H-1, (c) Co/H-2 and (d) Co/H-3 and EDS mapping of Co/Q-10 and Co/H-3 catalysts 30

Figure 13 TEM images of Co/Q-10, Co/H-3 and a zoom-in on the cobalt catalysts over SHS surface 32

Figure 14 H_2-TPR spectra of the Co/Q-10 and Co/SHS catalysts 33

Figure 15 XRD patterns of the Co/Q-10 and Co/H-3 catalysts after reduction at 400°C. 35

Figure 16 Catalytic performances for FTS on the Co/Q-10, Co/H-1, Co/H-2 and Co/H-3 catalysts 36

Figure 17 Product distributions over Co/Q-10 (left) and Co/H-3 (right) and the small models of the FTS reaction on the catalysts 37

Figure 18 XRD patterns of the prepared catalysts between using and without sonication 39

Figure 19 Product distributions over Co/Q-10 catalysts: sonication (left) and without sonication (right) 41

Figure 20 Nitrogen sorption isotherms of samples (a), pore size distribution of samples in mesoporous region (b) and micropore region (c) 42

Figure 21 XRD patterns of the Co/H-3 catalyst and the coated ZSM-5 over Co/H-3 catalysts of both coated methods 44

Figure 22 SEM images of samples: (a) Co/H-3/Z-coated and (b) Co/H-3/Z-SAC and EDS spectrum of (I) Co/H-3/Z-coated and (II) Co/H-3/Z-SAC catalysts 45

Figure 23 CO conversion of catalytic performance in FTS on the catalysts 46

Figure 24 Product distributions over the catalysts; (a) Co/H-3, (b) Co/H-3-coated, and (c) Co/H-3-sac 48

LIST OF TABLES

Table 1 Conventions of fuel names composition 6

Table 2 Most of all reaction in the FTS 6

Table 3 Summary of the chemical and textural properties of catalysts. 28

Table 4 Cobalt metal content and sodium contaminant in the catalysts. 31

Table 5 Amount of hydrogen uptake in the catalysts. 33

Table 6 Summary of the chemical and textural properties of catalysts. 35

Table 7 The FTS performance and distribution of products from the CO and H_2. 37

Table 8 Summary of the chemical and textural properties of catalysts. 40

Table 9 The FTS performance and distribution of products from the CO and H_2. 41

Table 10 Summary of the chemical and textural properties of catalysts. 45

Table 11 The FTS performance and distribution of products from the CO and H_2. 47

CHAPTER I

INTRODUCTION

1.1 Statement of problem

Currently, energy demand is higher from human consumption. But fossil energy source like coal, natural gas and crude oil will be disappeared in the near future. Biofuel is an interesting for an alternative energy. Agriculture wastes such as rice straw, fiber, palm bunch which are low cost and easy to find material are biomass. Biogas can be produced from biomass by gasification process and it will be transformed to be syngas ($CO+H_2$) by reforming process. Syngas can be changed to be hydrocarbon fuel by Fischer-Tropsch synthesis (FTS) [1, 2]. The FTS is an industrial process to synthesis of liquid hydrocarbons from hydrogenation of carbon monoxide. In FTS process, catalytic surface polymerization is applied to transform CO and H_2 to be Long-chain hydrocarbon as main product form reaction. Furthermore, small amount of branched hydrocarbon, unsaturated hydrocarbon and primary alcohol are also produced from reaction. Therefore, FTS is a good technique to produce gasoline (C_{5-11}) and diesel (C_{12-20}) ranges to instead petroleum fuel for transportation. Traditional FTS catalyst (such as Co, Fe, and Ni-based catalysts) is preferred to use cobalt as an efficiency catalyst with silica support because the cobalt based catalyst gives the highest yields, longest lifetime and produces supremely linear alkanes. Also, silicon oxide support has high surface area and good stability. Moreover, it shows less metal-support interaction compare to aluminum oxide and titanium oxide. Weaker metal-support interaction helps to get easily of Co species reduction [3, 4]. However, long chain hydrocarbon distribution through Anderson-Schulz-Flory (ASF) statistic can describe us on how level of secondary reaction of alpha-olefin cracking, reinsertion, readsorption and isomerizing to initiating hydrocarbon chain. The ASF distribution always shows broad peak and low selectivity which is depended on catalyst type and catalytic process. Heavy hydrocarbon deposition usually plugs at pore inside which causes catalyst deactivation. Most study observed hybrid between conventional catalyst and zeolite to get specific fuel with a narrow hydrocarbon distribution.

However, zeolite still gives catalyst deactivation. Furthermore, there are some disadvantage such as heat and mass transfer limitation for a fixed-bed reactor. Sheng et al. [5] presented on an effect of micro fibrous entrapped catalyst to avoid hot or cold spots in the catalyst bed and an increasing in product selectivity. Kanthana et al. [6] studied the FTS over Co supported on silica fiber catalyst which shows many advantages such as thermal stability, high surface area and efficient mass transport. Moreover, currently research are interested in many supports about hollow and mesoporous structures such as carbon nanotube [7, 8], multi-walled carbon nanotubes (MWCNTs) [8], carbon spheres (CSs) [9], SBA-15 [10, 11], MCM-41 [11], MCM-48 [12] and silica spheres [13, 14] for using in the FTS. There are many advantages of using the FTS including high accessibility of gas and hydrocarbon chains to an active phase, and an absence of micropore which leads to elimination of interparticle mass transferring. Xiong et al. [7] investigated an incipient wetness impregnation to prepare Co catalyst supported on carbon nanotube that showed the highest activity. Additionally, the C_{5+} hydrocarbon selectivity showed no observed change between inner and outer of pore confined carbon nanotube. Therefore, we are interested in mesoporous molecular sieve for using as catalyst support which is silica hollow sphere (SHS) called silica micro capsule. We select silica hollow sphere because it is synthesized by simple and inexpensive method. Moreover, the hollow sphere shape of SHS catalyst shows a silica wall at catalyst core which has steric restriction that can control chain length distribution in FTS reaction, avoiding catalyst deactivation.

The SHSs, developed by the National Institute of Advanced Industrial Science and Technology (AIST) [15], were produced by the reaction of sodium silicate as a silica source and NH_4HCO_3 as a silica precipitant in a water/oil/water (W/O/W) emulsion interface. The impregnated cobalt catalyst supported on SHSs that can satisfy all the requirements of a specific application has many advantages such as high surface to volume ratio, enhancing effective thermal conductivity and improving the chemical diffusion performances. That why we study on using cobalt-based SHS catalyst for the FTS to compare with commercial catalyst.

1.2 Studies of the thesis

The research schemes were carried out as follows:

1.2.1 Literature review.

1.2.2 Study of Fischer-Tropsch synthesis process in laboratory scale and analysis instruments.

1.2.3 Study of the characteristics of the silica hollow spheres.

1.2.4 Study the effect of physical and chemical properties of the catalyst based on the supports between commercial and silica hollow sphere supports in Fischer-Tropsch synthesis.

1.2.5 Study the combination of silica hollow sphere catalysts with zeolite and the catalytic performance in Fischer-Tropsch synthesis.

1.3 Objectives

1.3.1 Preparation of the cobalt based over silica hollow sphere catalyst.

1.3.2 Study of the catalytic activity of the cobalt based over silica hollow sphere catalyst in Fischer-Tropsch synthesis.

1.3.3 Study of the catalytic activity of the modified cobalt based over silica hollow sphere catalyst with ZSM-5 in Fischer-Tropsch synthesis.

CHAPTER II

THEORY AND LITERATURE REVIEWS

2.1 Overview of the Fischer-Tropsch synthesis

Recently, the interested in Fischer-Tropsch synthesis (FTS) [16, 17] that has grown up due to new alternative energy source replaced fossil energy source and green energy is a polymerization process on the surfaces of active phase catalyst. The FTS stream can produce several fuels that compose of various fuel types as listed in Table 1. The substrates in FTS consist of carbon monoxide (CO) and hydrogen (H_2) as known as syngas which is produced from coal, natural gas or biomass with reforming reaction. The syngas is formed by hydrogenation of adsorbed CO. The initiated CH_x monomers propagate to long chain length with continued adsorbed alkyl groups; the β-hydrogen of alkyl species can enter with abstraction to an olefin or hydrogen addition to generating n-paraffins until chain termination step or desorption of chain length hydrocarbon as shown in Figure 1. The readsorption of α-olefins start to reinitiation of hydrocarbon chain to the larger molecules or isomerization to the branched hydrocarbon which are secondary reaction. Molecular weight and kind of the hydrocarbon products are affected from secondary reactions which are possibly occur as olefin hydrogenation, hydrogenolysis and hydroformylation as shown in Figure 2.

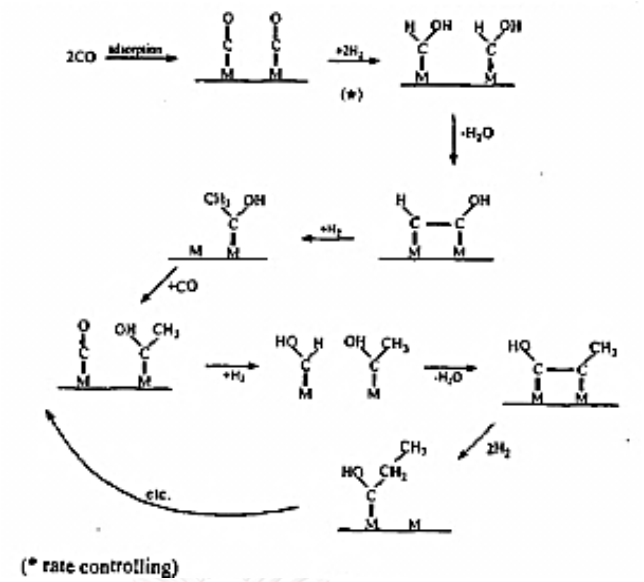

Figure 1 Schematic of the propagation to long-chain length [17]

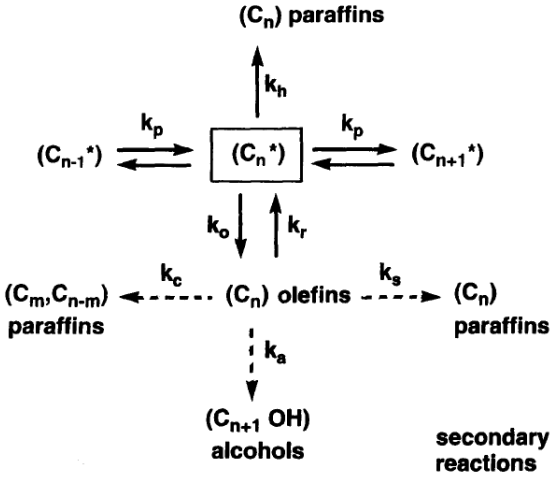

Figure 2 Chain growth pathways and possible secondary reactions of olefins in the FTS [16]

Table 1 Conventions of fuel names composition [4]

Name	Synonyms	Components
Fuel gas		C_1-C_2
LPG		C_3-C_4
Gasoline		C_5-C_{-12}
Naphtha		C_8-C_{12}
Kerosene	Jet fuel	C_{11}-C_{13}
Diesel	Fuel oil	C_{13}-C_{17}
Middle distillates	Light gas oil	C_{10}-C_{20}
Soft wax		C_{19}-C_{23}
Medium wax		C_{24}-C_{35}
Hard wax		C_{35+}

Therefore, the demand of the FTS products as hydrocarbon compound which have carbon atoms around 10-23 atoms. Main products are linear paraffins and α – olefin. Mostly reactions in FTS are summarized in Table 2. The generated products depend on type of catalyst, molar ratio of syngas, reaction condition, and so on.

Table 2 Most of all reaction in the FTS [4]

Main reactions	Paraffins Olefins Water gas shift reaction (WGS)	$(2n+1)H_2 + nCO \rightarrow C_nH_{2n+2} + nH_2O$ $2nH_2 + nCO \rightarrow C_nH_2 + nH_2O$ $CO + H_2O \leftrightarrow CO_2 + H_2$
Side reactions	Alcohols Boudouard reaction	$2nH_2 + nCO \rightarrow C_nH_{2n+2}O + (n-1)H_2O$ $2CO \rightarrow C + CO_2$
Catalyst modification	Catalyst oxidation/reduction Bulk carbide formation	$M_xO_y + yH_2 \leftrightarrow yH_2O + xM$ $M_xO_y + yCO \leftrightarrow yCO_2 + xM$ $yC + xM \leftrightarrow M_xC_y$

2.2 Effect factors of activity and selectivity for the FTS

The influence of the different catalyst types, size of particles and supports on the shape, appearance and, as well as on reducibility which affect to the performance in FTS.

2.2.1 Active sites

2.2.1.1 Types of active sites

The FTS reaction was designed to high activity, good selectivity and stability. Mostly common catalysts in FTS are group VIII metals as cobalt (Co), ruthenium (Ru), iron (Fe) and nickel (Ni) [18, 19]. However, the industrial factories prefer to use the cobalt and iron catalysts because the ruthenium catalyst is an expensive price and the nickel catalyst is low activity.

The cobalt catalyst gives the highest yields that means highest activity, the lifetime is longer than the others and it can produce predominantly linear alkanes. In a case of cobalt catalyst is widely applied in the homogeneous FTS process because of high activity and low cost. The iron catalyst, the FTS activity is lower than the cobalt catalyst, but there are many advantages such as the low cost, small byproduct as CH_4, low molecular weight hydrocarbon of paraffin and olefin products which can change to more alcohol and high water gas shift reaction. Moreover, the hydrocarbon chain of the iron catalyst is converted from syngas with a H_2/CO ratio. However, the cobalt catalyst gives a good straight long chain hydrocarbon which is transportation fuels such as gasoline, diesel, jet fuel, etc and more resistant to deactivation.

2.2.1.2 Cobalt catalyst particle sizes

The cobalt particle size in the range 3 to 18 nm on the FTS has influence to congenital activity and product distribution. Co metal is discovered to exist as Co_3O_4 on the calcined catalysts. Several research groups have reported about TOF decreasing for smaller cobalt particle sizes than 6-8 nm due to strong interaction between metal and oxide support, making higher catalyst dispersion result in difficult for reduction [20, 21], so the activity in FTS is almost independent on cobalt particle size with enough its large size in Figure 3. Moreover, the smaller cobalt particle size [22] is related to the

C_{5+} selectivity as shown in Figure 3. The selectivity was persistent for particles larger than 9–10 nm. Also, the C5+ selectivity directly relates with the CH_4 and C_2–C_4 selectivity. Thus, the least CH_4 and C_2–C_4 selectivity was also recorded at 8 nm in Figure 3 [20, 23].

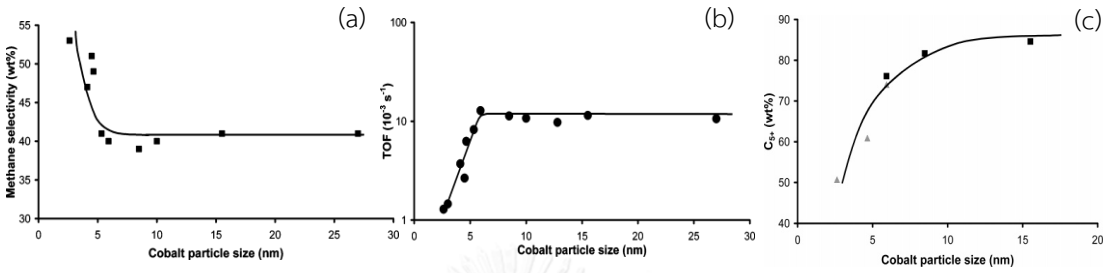

Figure 3 Influence of cobalt particle size on (a) the TOF at 35 bar and 210 ° C (b) the methane selectivity at 1 bar and 210 ° C, and (c) the C_{5+} selectivity at 35 bar with data markers in black at 210 ° C and in gray at 250 ° C [20]

2.2.1.3 Cobalt catalyst synthesis

The supported cobalt catalysts for FTS [22, 24] have several preparations such as impregnation, precipitation and co-precipitation, sol-gel preparations, etc. Each method may be applied and chosen for catalyst preparation about different chemical composition, so that allowing optimal dispersion and agglomeration of active sites, changed surface area and morphology after metal adding, etc.

The impregnation technique which is most common and simplest method is deposited cobalt on dried porous supports which is contacted with a cobalt precursor solution. There are two types of distinguish impregnation; incipient wetness impregnation (if not excess water in the pore volume) and wet impregnation (excess water more than pore volume). The wet impregnation is easier than the other because the solution is easily adjusted for suitable salt solubility, but it has some drawback such as solvent drying, making some metal holding on container, volume of solvent, stirring and so on. The incipient wetness impregnation is the most common method to prepare cobalt-supported catalysts which usually uses solutions of cobalt salt,

typically cobalt nitrate. When the cobalt precursor solution is drop on dry support after that the solution is transferred by the capillary forces to inner the pores of the support. Because the quantity of liquid is used equal the porous volume of support, leading full liquid and no excess moisture over that result in filling the pores. However, the incipient wetness impregnation is simple, requiring careful control of all impregnation parameters [24]: temperature and time of support drying, rate of addition of impregnating solution, temperature and time of drying, etc.

2.2.2 Texture of supports

The type and structure of the support for Co-supported catalysts influence the dispersion, particle size and reducibility, affecting the activity and C_{5+} selectivity [25].

2.2.2.1 Types of catalyst supports

In case of the cobalt catalyst is widely applied in homogeneous process in the FTS reaction due to its high activity. The homogenous catalyst has many drawbacks. Example, the catalysts need to be separated after reaction, it makes to increase pressure in during FTS reaction, and catalyst recovery may be difficult due to destroyed catalyst. Thus, recently many researches are interested in supported cobalt catalyst with increasing catalytic activity and selectivity. The catalyst supports as Al_2O_3, SiO_2, TiO_2 and ZrO_2 are used in the FTS because there are high surface area and strong mechanical strength [19, 22, 25]. There is some study on CO hydrogenation over Co catalysts supported on different supports that the specific activity of CO hydrogenation decreased in the order of Co/TiO_2>Co/SiO_2>Co/Al_2O_3>Co/C>Co/MgO. Moreover, the metal-support interactions affected the reduction of Co species, and the strength of such interactions decreased in the order Al_2O_3>TiO_2> SiO_2.

Silica support as a common support catalyst is used in FTS, presenting the characteristics of a higher surface area, porosity, stability and weaker metal–support interaction than the others as above mentioned. But, the weak interaction between cobalt and silica support favors to agglomerate of supported cobalt particles, reducing the dispersion of cobalt based on silica support.

Alumina support is an employed support for cobalt FTS catalysts due to favorable mechanical properties and adjustable surface properties. However, unlike the cobalt silica catalyst, the cobalt alumina catalysts have more acidity, leading to cracking and isomerizing, lower chain growth probability, and higher selectivity to lighter hydrocarbons, but limited reducibility and diffusion of the cobalt metal on support [19, 25].

If the target of production is gasoline product, using the cobalt supported on zeolite support catalysts is to be preferred as a lighter, more highly branched. The ZSM-5 is a good support for cobalt catalyst for desired high octane gasoline product [25]. But the activity of the catalyst over zeolite is decreased with time on stream because of the poisoning of the acid sites by coke deposition [4].

2.2.2.2 Pore size of catalyst support

The Co_3O_4 particle size, Co^0 particle size, and reducibility can increase with an increasing an average pore diameter of the support as shown relation of them in Figure 4 [22, 26, 27]. Khodakov et al. [27] found the smaller particles in the narrow pores (2-5 nm) are more difficult to reduce Co_3O_4 to Co metal species than larger particles situated in the broad pores (>5 nm) of mesoporous silicas. Also, the larger diameter of pores led to significantly higher C_{5+} selectivity [28].

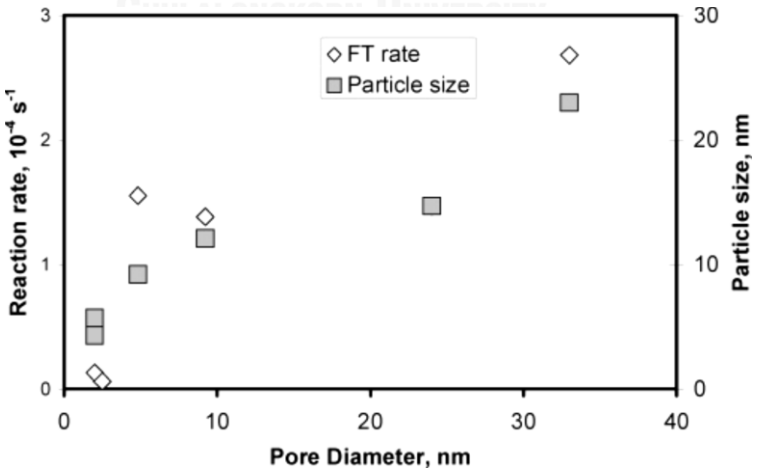

Figure 4 Relation between pore diameters, sizes of supported Co_3O_4 particles, and FTS reaction rates over cobalt catalysts supported by mesoporous silicas [22]

2.2.2.3 Hybrid catalyst

The development of catalysts in the FTS has been studied for the increase amount of transportation fuels as gasoline, diesel and jet fuels. Currently, the FTS catalysts are improved by a combination of the catalyst and other metals or the catalysts with acidic zeolites. For the extend isoparaffin products in the gasoline range, which the hybrid catalysts can produce [4]. The hybrid FTS catalyst is physical combination of two components together, has been improved to be applied to the FTS and hydrocracking reactions simultaneously within a single reactor because the common FTS catalyst has function about chain polymerization and termination during reaction as the first step, and the zeolites have acid sites for hydrocracking and isomerization in the second step. Conclusion, the use zeolites as support catalyst has deactivation as above mentioned; however, there is proper temperature for zeolite catalyst working [29] or addition of the promoters which can suppress the deactivation [4]. Then, the mixing of FTS catalyst and zeolite as hybrid catalyst that can improve the target product. Nevertheless, the hybrid catalyst has the drawback; a two-stage reactor is designed for normal FTS reaction and the second reaction. For decrease investment, the encapsulated H-ZSM-5 zeolite coated Co/SiO_2 catalyst [29] is proposed that shows lower C_{11+} hydrocarbons in Figure 5, while physical-mixed catalyst still has a lot of C_{11}–C_{25} products [30]. Moreover, the developed zeolite membrane coating was prepared by using steam-assisted crystallization (SAC) process as shown in Figure 6. The SAC process as the coated zeolite for improvement zeolite coating because the hydrothermal synthesis has problem producing a lot of waste water and limitation design of the shell-coated core catalysts. In case of the physical adhesive method had not independent the core catalysts were directly contacted with zeolite powders and very low gasoline selectivity [30].

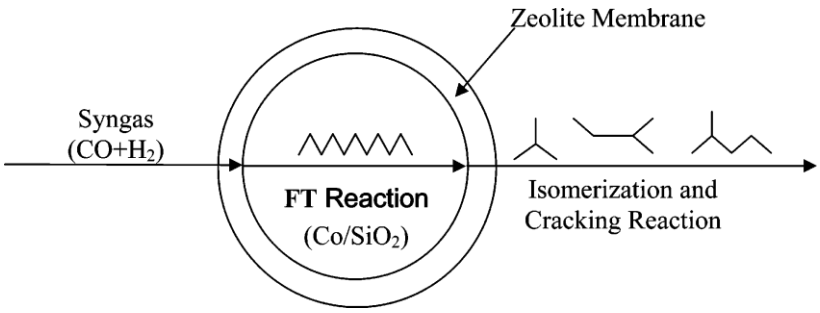

Figure 5 Schematic image of the capsule catalyst role in the FTS reaction [29]

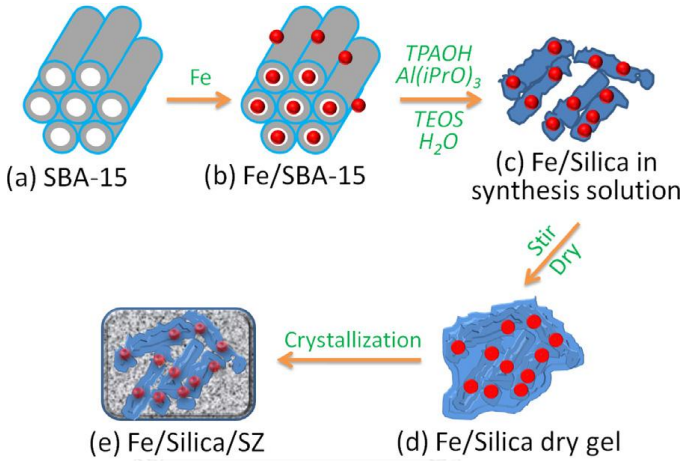

Figure 6 Synthesis schematic route of iron-based micro-capsule catalyst in SAC process [30]

2.2.2.4 Mesoporous materials

Currently, many researches are interested about the mesoporous material is a material containing pores with diameters between 2 and 50 nm due to the characteristic of the mesoporous structure in reducing the mass transfer limitation of heavy reactants. In the FTS reaction has natural problems of the wax deposition on the active phases and changing activity due to the deposited liquid-phase heavy hydrocarbons, causing to diffusion rate of syngas through the nonpolar heavy hydrocarbon layers. Therefore, these materials can solve these problems in FTS, including the high accessibility of gasses and hydrocarbon chain to the active phase; moreover, the absence of any micropore, thus eliminating of mass transferring

interparticle [9, 31, 32]. For examples, Carbon nanotube [7, 8], multi-walled carbon nanotubes (MWCNTs) [33] and carbon spheres (CSs) [9] and mesoporous silica such as SBA-15 [10, 11], MCM-41[11], MCM-48 [12] and silica spheres [13, 14] which the silica hollow spheres actually were prepared with the surfactants for template to be core-shell via the emulsion process which were simple and inexpensive method.

2.2.3 Reaction conditions; Temperature, Gas Hourly Space Velocity, Syngas ratio and Total pressure

2.2.3.1 Temperature

The temperature increases as stated in thermodynamics makes more light products. However, very few studies are interested in different temperatures during the FTS reaction, there is one example of a patent has been regenerated in Figure 7 that shows the temperature effect is expected to be a constant CO conversion, but it increases. At the same time, the C_{5+} selectivity decreases that probably a water vapor pressure increases due to the generated byproduct as water that suppresses the hydrogenation rate during the FTS reaction [34].

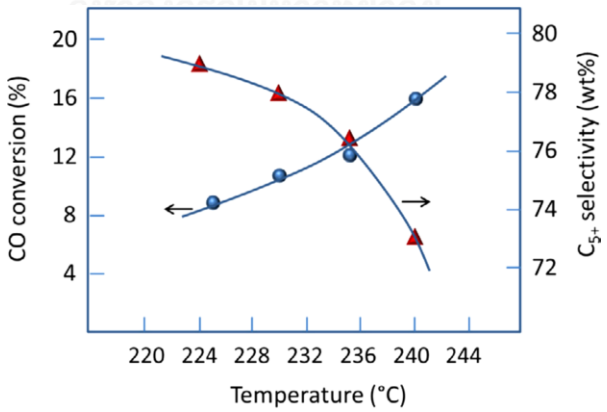

Figure 7 Effect of temperature on C_{5+}selectivity for a Co/Ru/alumina catalyst operated in a slurry reactor [34]

2.2.3.2 Syngas ratio and Total pressure

Supposedly, when the H_2/CO ratio increases, making more the adsorbed hydrogen atoms on the cobalt surface catalyst and lower *CH_2 radical than the less H_2/CO ratio. Thus, the higher H_2/CO ratio affects to hydrogen addition, more methane and saturated chains as the shorter chain hydrocarbons. The commercial operations use the H_2/CO ratio below 2 about 1.95-1.98. Additionally, when the pressure is increased from 10-30 bar, only the methane selectivity slightly reduce so enhanced pressure can improve the selectivity. However, the effect of pressure with conversion is discussed by Yang et al. [35] that found an effect of pressure from 20 to 40 bar in microreactor experiments at 210°C, but no effect at 225°C. Conclusion, there is no common trend of pressure, but it will be needed to explain the pressure effect of the system within reach. In case of the iron catalysts can also use syngas with the H_2/CO ratio below 2, because of the WGS activity. A lot of carbon monoxide is changed with water to carbon dioxide and hydrogen.

2.2.3.3 Gas Hourly Space Velocity

Gas Hourly Space Velocity (GHSV) is usually used on constant in many reports, meaning constant conversion [34, 36]. Besides, studying about comparing of different catalysts has been indicated comparative studies on FT selectivity. If decreasing GHSV as increasing the residence time, there is longer interaction between active sites on catalysts and the gas molecules leading to higher carbon monoxide conversion, also long chain products due to further hydrogenation and oligomerization of short–chain hydrocarbons. Therefore, the GHSV should keeping for same effect and the conversion can be varied by changing about the catalysts.

2.2.4 Reactors

Many reactor types have been suggested in the FTS process [37, 38]. The common reactors in for industrial factory use fixed-bed and slurry bubble reactors for low temperature FTS but each of them suffers from some drawbacks which are challenging engineering problems.

2.2.4.1 Slurry-phase reactor

Slurry-phase reactor in Figure 8 which shows advanced reactor technology for gas-to-liquid process is one type of the commercial reactor for the middle distillates production [37, 39]. Syngas is bubbled through the slurry of catalyst particles and heavy liquid products in the reactor. Unreacted syngas and light products leave the reactor in the gas phase, while the liquid products are contained in a part of the slurry. Its advantages include simple construction, superior heat transfer performance and good temperature control which make it very suitable for gas-to-liquid processes [39]. But, its complexity about multiphase flow behaviors under industrial conditions affects to limitations in gas-liquid-solid slurry systems which consist of the high temperature, pressure, and solid concentration may cause a decrease conversion due to the bubble behaviors, gas holdup, liquid velocity, mass and heat transfer behaviors. Moreover, the separation of spent catalyst particles from the viscous wax in FTS is a problem. Therefore, the fixed-bed reactor is interested for an alternative in the commercial FTS reactor

2.2.4.2 Fixed-bed reactor

The fixed-bed reactor is easier and cheaper than the slurry-phase reactor, so it is usually chosen for the FTS process. The catalyst pellets in the fixed-bed reactor are held in place and do not move at the core part of the packed-beds reactor where the reaction takes place [25, 37, 40]. Heat removing has been the major issue in these technologies, causing low productivities. The hydrocarbon selectivity is dependent on the reaction temperature, leading the developing of the fixed-bed reactor as the multitubular fixed-bed reactor as shown in Figure 8 for solving the heat removing problems, but an increasing complexity of system leads to higher cost. Moreover, there

is the limitation in the fixed-bed technology about using too small catalyst particle size that results in a high pressure drop over the reactor and, the distribution of gas and liquid over a lot of parallel tubes is not direct due to catalyst packing and flow resistance which essentially relate to catalytic activity, selectivity, and stability. Therefore, the presenting of the slurry column has considerable solving this problem. However, the slurry reactor has a higher cost than the fixed-bed reactor, and the catalyst in the slurry process cannot be calcined and reduced with hydrogen in situ. It needs to pretreat about H_2 reduction ex-situ and passivation after that can bring in the reactor. Therefore, period of organizations of the slurry reactor is more than fixed-bed reactor

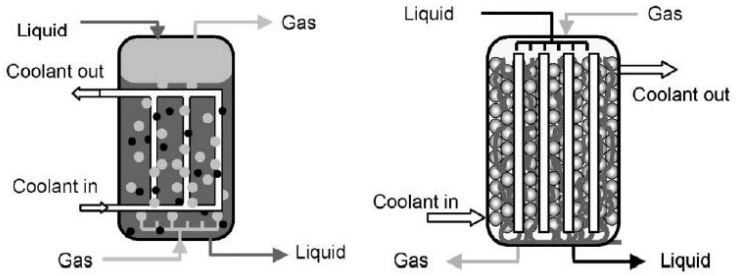

Figure 8 Schematic of FTS reactor type used commercially between slurry-phase reactor (left) and multitubular fixed-bed reactor (right) [37]

Relationship of the catalysts in fixed-bed reactors shows some limitations as plug flow hydrodynamics, mass transfer: intraparticle and external, heat transfer and hot spot [21]. There is plug flow hydrodynamic in fixed-bed reactor, but no concentration gradients should be showed inner the catalyst particle. In case of intraparticle mass transfer limitation about transportation of reactants or products in the catalyst particle is not enough fast for chemical reaction, leading to lower CO conversion and affect hydrocarbon selectivity. The mass transport inside the pore catalyst which is known that diffusion of gas and liquid depend on temperature, pressure and composition of reactants. Additionally, the geometry, porosity and tortuosity of the catalyst, also the diffusion ability of the reactants and products effect of mass transport inside the porous catalyst. Moreover, the various catalyst particle

sizes have an influence of intraparticle mass transfer and pressure drop. Many experiment and computation recommend that using the particle size between 50-200 μm, indicating no internal limitations. The intraparticle diffusion influences hydrocarbon selectivity more than CO conversion because a higher H_2/CO ratio inside the particle, a higher probability of methanation. Moreover, the WGS enhances rate reaction due to generated water during FTS reaction and larger pellet size, making difficult in being removed from the center to the outer surface of the catalyst.

The mass transfer limitations for external catalyst particles or between gaseous and liquid phases may affect to the activity and selectivity in the FTS. Also, the mixed catalyst and inert material in the fixed bed reactor for keeping plug flow may lead to bypassing and decrease the catalytic activity.

The heat transfer can influence in the fixed bed reactor due to highly exothermic from the FTS. The gaseous phase is lower heat conductivity, leading to axial and radial temperature gradients in the reactor. The different temperatures on the outer surface and inside the catalyst particles can be shown, so somewhere has high heat in the catalyst layers where mostly syngases can be converted, but in other part that is significantly less heat of the fixed bed reactor can produce lower. The inert materials can reduce the temperature gradient in the catalyst bed.

2.2.5 Other deactivation parameters

Causes of catalyst deactivation in Fischer–Tropsch synthesis, such as contamination of alkali and alkaline earth metals, sintering of cobalt crystallites, re-oxidation, metal–support solid state reactions and so on, leading the decrease catalytic activity [21].

2.2.5.1 Alkali and alkaline earth metals

The alkali and alkaline earth metals, i.e. Na, K, Li affect to the FTS catalyst behavior. When alkali metal is added, adversely influencing the catalytic activity, but the chain growth probability increases significantly. Therefore, the alkali metal is offered that should have optimum concentration level for balancing of activity and

selectivity. At any rate, the poisoning of alkali metals cannot obviously operate about deactivation mechanism.

2.2.5.2 Sintering of cobalt crystallites

The active surface area is reduced by sintering effect which is thermodynamically moved due to energy minimization interaction between support and metal, leading the different size due to dependent mobility of the crystals on various supports significantly. However, there is dispersion again (redispersion) through reduction-oxidation-reduction treatment causes the catalytic activity like beginning activity, so the deactivation in the FTS can occur by other effects, not always sintering.

2.2.5.3 Re-oxidation

The catalyst deactivation is the possible re-oxidation of cobalt metal during the reaction, and becoming inactive sites. There are many oxidizing agents from the byproducts and water of the FTS. The water is produced from common FTS reaction and side reaction of surface oxygen and hydroxyl species by hydrogenation on the surface.

2.3 Literature reviews

Tessonnier et al. [32] studied deposition of metal nanoparticles on MW-CNTs between inside and outside supports which prepared by two-step biphasic impregnation of the organic and aqueous solvents with capillary force, when a dry porous support is contacted with a filled solution of metal in salt solution and after that the solution is desired to enter inside the pores with no moisture in these pores by vacuum

Xiong et al. [7] studied the shape of carbon material such as carbon nanofibers (CNFs), carbon nanotubes (CNTs) and carbon micro-coils (CMCs). The cobalt catalysts were prepared by incipient wetness impregnation on these supports sited both in and out of porous catalyst which are influenced different appearance, size and dispersion of cobalt particles. The FTS performance of Co/CNT-in catalyst was showed higher

catalytic activity than the Co/CNT-out due to higher reducibility and dispersion. However, the C_{5+} selectivity is not different both Co/CNT-in and Co/CNT-out catalysts.

Zhu et al. [33] observed the cobalt catalysts were located on the internal or external surface of multiwall carbon nanotube (MW-CNTs) which are no significant difference in the catalytic C_{5+} selectivity through the FTS reaction, pretreated at 400°C. Also, suggesting both internal and external surface are different electronic density which do not significantly affect the selectivity hydrocarbons on cobalt supported catalysts.

Xiong et al. [9] studied the cobalt catalysts on carbon nanotubes (CNT) and carbon spheres (CS). The reduction catalysts for FTS activity, if using pure H_2 is proper at 400°C, using under N_2 is better at 480°C. And, the CSs preparation was easier than CNTs. The TOF of both catalysts was constant when cobalt particles size above 10 nm.

Xiong et al. [10] studied the role of different pore size for Co/SBA-15 by incipient wetness impregnation. In the TPR analysis indicated the second stage reduction of CoO → Co^0 that was much easier on the larger pore of catalysts. The larger pore of catalysts led to larger cobalt cluster size, lower dispersion, and higher reducibility. However, the larger pore gave higher CO conversion and then lower when decreased pore size in the range studied. The C_{5+} selectivity was increased with larger cobalt cluster size.

Gonzalez et al. [11] studied the cobalt catalysts based on mesoporous silica, SBA-15, Al-MCM-41, INT-MM1 and commercial amorphous silica. The catalyst with larger cobalt oxide phases located in wide pore silica showed that to be easily reducible, more active and higher diesel selectivity. The Co/SBA-15 showed the most activity, more C_{5+} selectivity and less CH_4 selectivity while Al-MCM-41 and INT-MM1 were used as the support, gave lower CO conversion, C_{5+} selectivity, but high CH_4 selectivity because of reduced pore size, leading to smaller cobalt cluster size.

Hualan et al. [12] studied MCM-48 as support of the cobalt catalyst for FTS that prepared by incipient wetness impregnation with various cobalt loading 5, 10 and 15wt%. The Co loading 5wt% is less CO conversion and C_{5+} selectivity than others due

to lower reducibility of smaller cobalt particles, while the cobalt was loaded exceeding 10 wt%, showing no significant effect on FTS properties of the catalysts.

Li et al. [13] studied the cobalt based on hollow mesoporous silica spheres with bimodal pore distribution were prepared by the two-solvent method which showed the cobalt particles located inside the pore of silica spheres. The small cobalt loading showed small cobalt particles, leading to easily reoxidized by water and other byproducts and higher methane selectivity while increasing cobalt loading represented bigger cobalt crystallite sizes that causes to good catalytic activity and high C_{5+} selectivity. Therefore, the hollow structure simplifies reactants to enter the active sites.

Subramanian et al. [14] studied the encapsulation cobalt nanoparticles in nanosized porous silica spheres because the FTS hydrocarbon products were the broad distribution in the cobalt catalysts. So, the improved catalyst resolves this problem by the limitation of chain growth in the core of the catalyst capsules.

He et al. [29] improved the isoparaffin selectivity in the FTS with the capsule catalyst by coating H-ZSM5 membrane on commercial Co/SiO_2 with hydrothermal synthesis due to acid sites on the zeolite for hydrocracking and isomerizing.

Xing et al. [30] developed zeolite membrane coating was prepared by using steam-assisted crystallization (SAC) process. Usually, the coated zeolite was prepared by hydrothermal synthesis or physical adhesive method, but the hydrothermal synthesis has the problem producing a lot of waste water and limitation design of the shell-coated core catalysts. In case of the physical adhesive method had not independent the core catalysts were directly contacted with zeolite powders and very low gasoline selectivity. Therefore, the SAC process was the new method for coating zeolite and good catalytic performance for high selectivity of isoparaffin synthesis.

CHAPTER III

EXPERIMENTAL

3.1 Materials and reagents

1. Silica (Cariact Q-10), Fuji silysia chemical
2. Cobalt nitrate hexahydrate, Wako pure chemical
3. ZSM-5, Sud-Chemie catalyst
4. Nitrogen gas (99.99% purity), Praxair
5. Hydrogen gas (99.99% purity), Praxair
6. Hydrogen gas/Carbon monoxide gas (H_2/CO) 2:1, BOC Scientific
7. Argon gas (99.99% purity), Praxair
8. Standard gas; 20% of CO, 20% of CH_4 and 20%H_2balanced He, BOC Scientific
9. Standard gas 100 % of CO_2, Praxair

3.2 Catalyst preparation

3.2.1 Silica hollow sphere (SHS) preparation

The SHS supports with different surface areas which were produced by the National Institute of Advanced Industrial Science and Technology (AIST) [15]. In a typical procedure, the aqueous solution of sodium silicate (Water glass No.3 purchased from Kishida Chemical) was added to n-hexane solution with Tween 85, and the resulting two phase solution was emulsified at by a homogenizer (IKA-T25 digital ULTRA-TURRAX). This W/O emulsion was immediately poured into the aqueous solution of NH_4HCO_3 with stirring at 400 rpm. After 10 min stirring, the precipitated solid was filtered, washed with deionized water three times and methanol, and dried at 120 ° C for 12 h. The prepared SHS supports were denoted as H-1, H-2, and H-3 which

represented different surface area as 430, 453, and 506 m^2/g, respectively as shown in Table 3.

3.2.2 Preparation of supported cobalt catalysts

The series of cobalt over SHS support catalysts were prepared by incipient wetness impregnation method as followed. Firstly, $Co(NO_3).6H_2O$ was dissolved in distilled water. Then, the prepared precursor was impregnated on supports after that vacuum for 2 h. And the prepared catalysts were dried at 120 ° C overnight and calcined at 400 ° C for 2 h at a heating rate of 2 ° C/min. The samples are labeled as Co/H-1, Co/H-2, and Co/H-3. Moreover, comparison with a commercial catalyst as silica support Q-10 (size of 0.075-0.15 mm) denoted as Co/Q-10. The Co amounts of the catalysts were loaded of 10%wt.

3.2.3 Preparation of zeolite membrane coating on SHS

The SHS catalyst which was improved the specific selectivity of gasoline range (C_{5-11}) was coated with ZSM-5 on the Co/SHS catalyst as provided a good activity in FTS reaction because the first step of the reaction had propagation of long chain hydrocarbon on active sites and the second step had hydrocracking and isomerizing on acid sites of zeolite. This research was interested about ZSM-5 coating with two methods which were hydrothermal method and steam-assisted crystallization process.

3.2.3.1 Hydrothermal method

The coated H-ZSM-5 zeolite over the cobalt on silica hollow catalyst was prepared by hydrothermal synthesis and denoted as Co/H-3/Z-coated. Firstly, 0.5 g of Co/H-3 was added to zeolite precursor solution (molar ratio of TEOS: 0.25TPAOH: $60H_2O$:4EtOH:$0.0125Al_2O_3$) were mixed and sealed in a Teflon lined autoclave at 180 ° C for 48 h. The sample was washed with distilled water for several times, filtrated and dried at 120 ° C overnight. Lastly, the dried sample was calcined at 500 ° C in air for 5 h that obtained the Co/H-3/Z-coated.

3.2.3.2 Steam-assisted crystallization (SAC) process

The cobalt on silica hollow catalyst as core and H-ZSM-5 zeolite as shell were prepared by using an in-situ crystallization route via steam-assisted crystallization (SAC) process and denoted as Co/H-3/Z-sac. Firstly, 1 g of Co/H-3 was added to a mixture of aluminum isopropoxide, distilled water, and TEOS under vigorous stirring until getting a sol. Then, tetrapropyl ammonium hydroxide (TPAOH, 10%) was added dropwise into the sol. The wet gel was aged at 60°C for 8 h after that dried at 90°C for 12 h. Next, the as-prepared gel was crystallized by hydrothermal synthesis method at 160°C for 18 h. The sample was washed with water for several times, filtrated and dried at 120°C overnight. Lastly, the dried sample was calcined at 500 ° C in air for 5 h that obtained the Co/H-3/Z-sac with the final molar ratio Of Al_2O_3:SiO_2:H_2O: TPAOH of 0.008: 1: 38: 0.01.

3.4 Catalyst characterization

3.4.1 N_2 physisorption

The structures of catalysts such as surface area, pore diameter, and pore volume were characterized by N_2-sorption analysis with 3 Flex analyzer (Micromeritics Instrument Co.) Before analysis, the samples were degassed at 200°C for 2 h. The surface area of samples was calculated by the BET method. The pore size distribution in the mesoporous region was obtained by BJH method from the desorption branch of the isotherms, and the microporous region was analyzed by the HK method. Also, the surface area and volume of micropore were measured by the t-plot method.

3.4.2 X-ray diffraction (XRD)

The chemical structures of catalysts were characterized by XRD with a Rigaku RINT 2200 X-ray powder diffractometer using monochromatized Cu-Kα radiation and scanned at 40 kV and 40 mA. The average Co_3O_4 particle sizes were estimated by Sherrer equation using a Co_3O_4 peak at 2θ = 36.8°.

3.4.3 Scanning electron microscopy and energy dispersive spectroscopy (SEM-EDS)

The morphology of supports was characterized by SEM (JEOL, JSM-6360LV). The determination of the amount of metal content in each catalyst was performed using EDS.

3.4.5 Transmission electron microscopy (TEM)

The structures of supports and the component of cobalt particles on supports were examined by TEM (TOPCON 002B with the acceleration voltage of 120kV). The sample for TEM analysis was prepared in ethanol with sonication for 10 min. The prepared sample was dropped onto a copper grid and dried at room temperature.

3.4.6 H_2-Temperature-programmed reduction (H_2-TPR)

The reducibility of the supported metal oxide phases was studied by H_2-TPR in a BELCAT-B-TT instrument. About 50 mg of a sample using 5% H_2 diluted by Ar at an atmospheric pressure. The pretreated catalyst sample was heated to 200°C in flowing Ar for 1 h. Subsequently, the 5% H_2 (30 ml/min) was introduced into the catalyst sample, and then linearly raised the temperature from 40°C to 850°C at a rate of 5.0° C /min. The H_2 consumption was monitored by a thermal conductivity detector (TCD).

3.5 FTS reaction performance

The FTS performance of catalysts was tested in the fixed-bed reactor with H_2/CO molar ratio of 2, reaction temperature of 240° C, W/F of 10 ghmol^{-1} and a reaction pressure of 1.0 MPa for 6 h. The effluent gas from a reactor was analyzed by two online gas chromatographs. The Ar, CO, CH_4, and CO_2 were analyzed by thermal

conductivity detector (TCD) with an active charcoal column and the C_1-C_8 hydrocarbons were analyzed by flame ionized detector (FID) with the Porapak-Q column. The liquid products were collected in ice trap and then analyzed by an off-line FID in a Shimadzu GC-2014 gas chromatograph (Inertcap 5 capillary column). Before the FTS reaction was carried out, the cobalt metal oxide was reduced in pure hydrogen gas with a temperature of 400 ° C for 10 h.

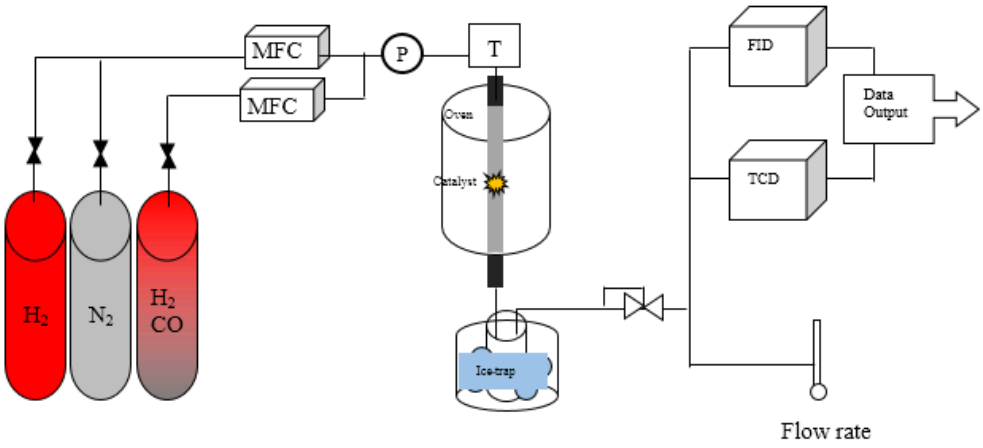

Figure 9 Schematic of FTS system

CHAPTER IV

RESULTS AND DISCUSSION

4.1 Comparisons between Co based commercial silica and SHSs.

4.1.1 Structural and textural of catalysts.

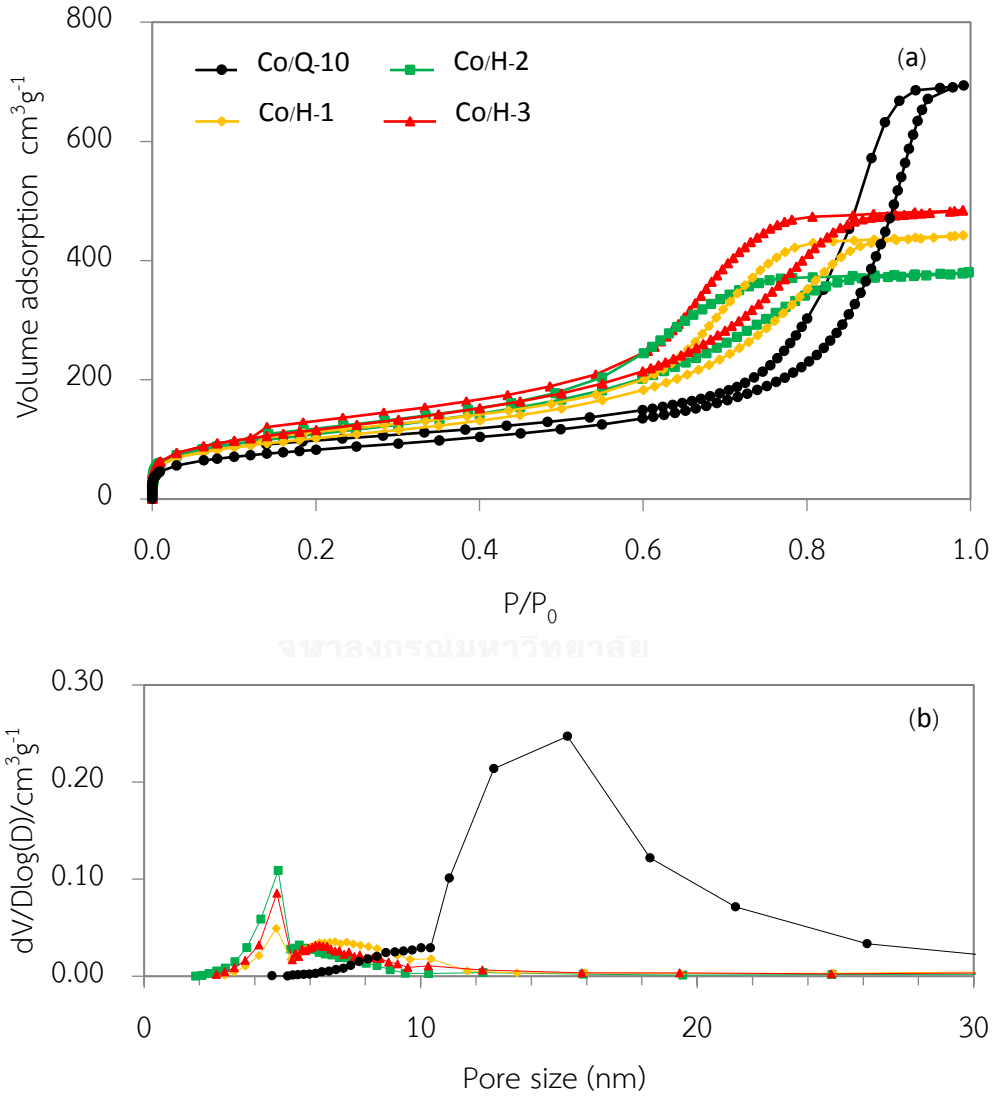

Figure 10 Nitrogen sorption isotherms of samples (a) and pore size distribution of samples in mesoporous region (b)

The nitrogen adsorption and desorption isotherm are represented in Figure 10 (a). All cobalt-based SHS catalysts exhibit type-IV isotherms with H1 hysteresis loops, suggesting tubular mesopore structures which are like the commercial silica support. Nevertheless, the adsorption capacity of nitrogen in SHS pores is lower than commercial catalyst, indicating smaller pores [41]. The pore size distribution (PSD) of all catalysts obtained by using the BJH method is shown in Figure 10 (b). The SHS catalysts have bimodal pore distribution around 5 and 7 nm in mesoporous region. Moreover, the specific surface area, pore volume, and pore size are summarized in Table 3. The surface area and pore volume of impregnated cobalt catalysts on supports are decreased while the pore size of impregnated supports are the same size as fresh supports, suggesting the access of cobalt species inside the support pores. Also, the cobalt oxide particles possibly locate inside the core of SHS support. Tessonnier et al. Tessonnier, Ersen [32] believed that the incipient wetness impregnation process could conduct Ni precursor aqueous solution into the channel by capillary force. Therefore, a porous silica support contacted with a solution of cobalt nitrate, leading to entering of the solution to the pores [22, 28, 42, 43]. Moreover, the Co/H-3 catalyst has less micropore in silica support. Small amount of micropore results in the elimination of diffusion and plugging of products inside the micropore that is one part of the deactivation effect [10].

Table 3 Summary of the chemical and textural properties of catalysts.

Catalysts	S (m^2/g)			Pore volume (cm^3/g)[c]	Average pore size (nm)	Co_3O_4 particle size (nm)[d]
	Total	Micropore[a]	Mesopore[b]			
Q-10	326	31	295	1.20	14.8	-
H-1	430	36	394	0.85	7.9	-
H-2	453	21	432	0.73	6.5	-
H-3	506	17	489	0.88	7.0	-
Co/Q-10	295	29	266	1.07	14.5	13.2
Co/H-1	366	26	340	0.69	7.5	9.7
Co/H-2	392	19	373	0.59	6.0	8.8
Co/H-3	420	10	410	0.75	7.1	9.2

[a]Microporous surface area evaluated by the t-plot method.

[b]Mesoporous surface evaluated by the t-plot method.

[c]Pore volume calculated by the single point method at $P/P_0 = 0.99$.

[d]Co_3O_4 particle size calculated by the Scherrer's equation.

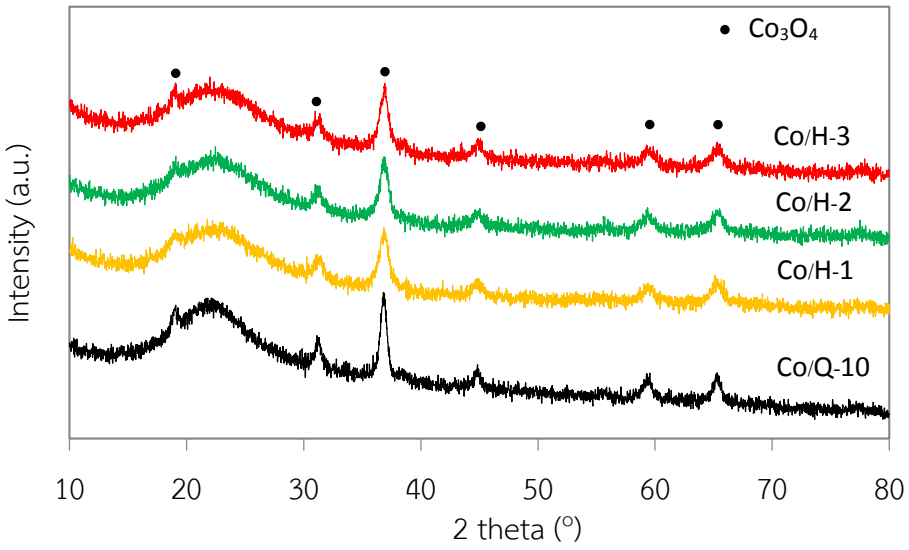

Figure 11 XRD patterns of the catalysts

The XRD patterns of the Co/SHS catalysts demonstrate the located peak of Co_3O_4 crystalline phase at 2θ of 19.0°, 31.3°, 36.8°, 44.7°, 59.4° and 65.2° (Figure 11). Also, the broad peak at 22.5° is attributed by amorphous silica [6]. The Co_3O_4 crystallite sizes of the Co/Q-10, Co/H-1, Co/H-2 and Co/H-3 catalysts are calculated by widths of the most intense diffraction peak at 2θ = 36.8° using the Scherrer's equation, which are 13.2, 9.7, 8.8 and 9.2 nm, respectively. Table 3 represents the size of Co_3O_4 crystallites, which depend on the average pore diameters in mesoporses; wider pores in silica supports are observed the larger Co_3O_4. So, the Co_3O_4 crystallite size of Co/Q-10 catalyst is the biggest size due to the largest pore diameter [28, 44, 45]. The cobalt cluster size is an important factor in part of catalytic activity [21], but their sizes of cobalt catalysts are similarly large enough to exhibit an insignificant effect on catalytic performance in FTS reaction [22, 43].

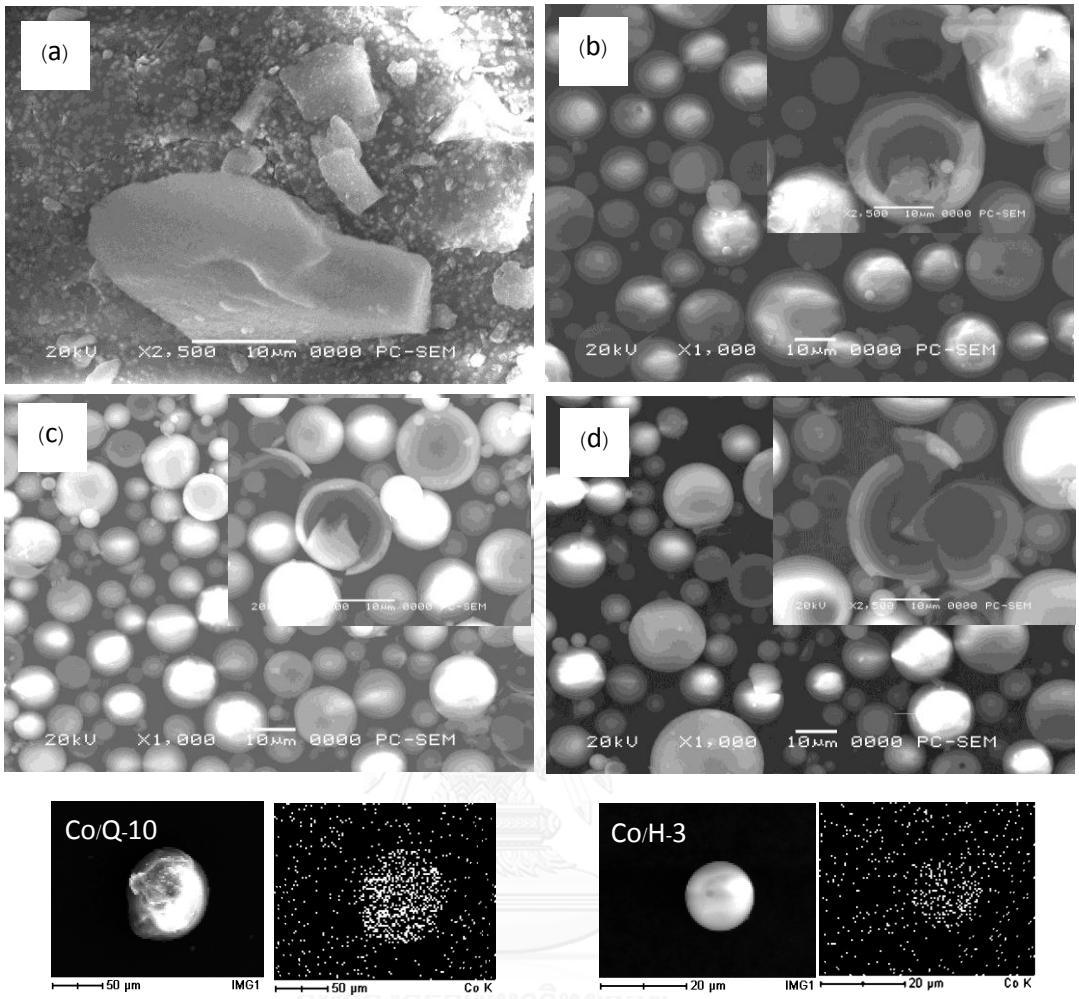

Figure 12 SEM images of samples: (a) Co/Q-10, (b) Co/H-1, (c) Co/H-2 and (d) Co/H-3 and EDS mapping of Co/Q-10 and Co/H-3 catalysts

The SEM images of SHS catalysts are shown in Figure 12 (b-d). The SEM images shows that spherical shape and core-shell structure of the Co/SHS compared with the Co/Q-10. The EDS mapping images in Figure 12 report the result of the elemental dispersion of the doped silica support. The Co dispersion on the Co/Q-10 and Co/H-3 is similar pattern. The element mapping images represent the cobalt catalysts which are prepared by wetness impregnation method dispersed on surface of supports.

Table 4 Cobalt metal content and sodium contaminant in the catalysts.

Catalysts	Co content (%wt)[a]	Na content (%wt)[a]
Co/Q-10	12.5	0.11
Co/H-1	11.7	0.09
Co/H-2	10.0	0.06
Co/H-3	12.3	0.07

[a]analyzed from EDS

The metal amount is analyzed by EDS analysis as shown in Table 4. These catalysts were prepared by the incipient wetness impregnation, which cobalt loading was 10%wt. The SHS support were prepared using the water-in-oil-in-water (W/O/W) multiple emulsions method, which were employed to synthesize using sodium silicate as silica source. The contamination of sodium in catalysts tends to decrease catalytic activity during the FTS reaction. EDS analysis (Table 4) shows almost the absence of sodium in the catalyst. Therefore, the observed sodium content is not significant effects during FTS reaction.

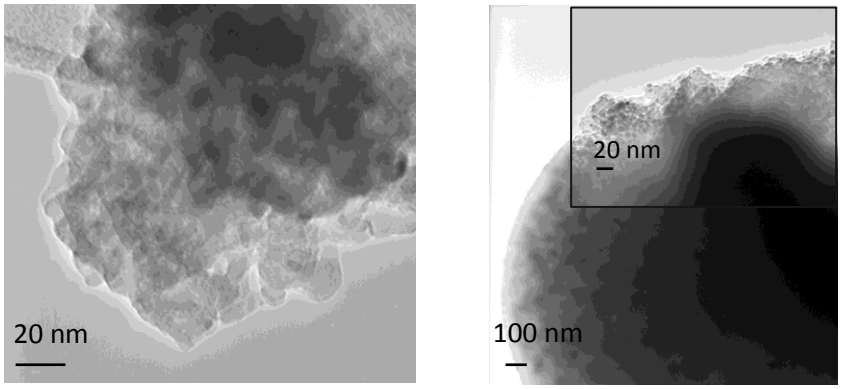

Figure 13 TEM images of Co/Q-10, Co/H-3 and a zoom-in on the cobalt catalysts over SHS surface

Figure 13 shows TEM images of the calcined Co/Q-10 and Co/H-3 catalysts. The dark spots indicate the cobalt species dispersing on the silica support. The TEM image of Co/Q-10 represents a nonuniform distribution of the metal nanoparticles (Figure 13). The Co_3O_4 particle size of Co/Q-10 accordance with the XRD analysis was larger with the average size about 13.2 nm while the average size of cobalt oxide crystalline of Co/H-3 was 9.2 nm.

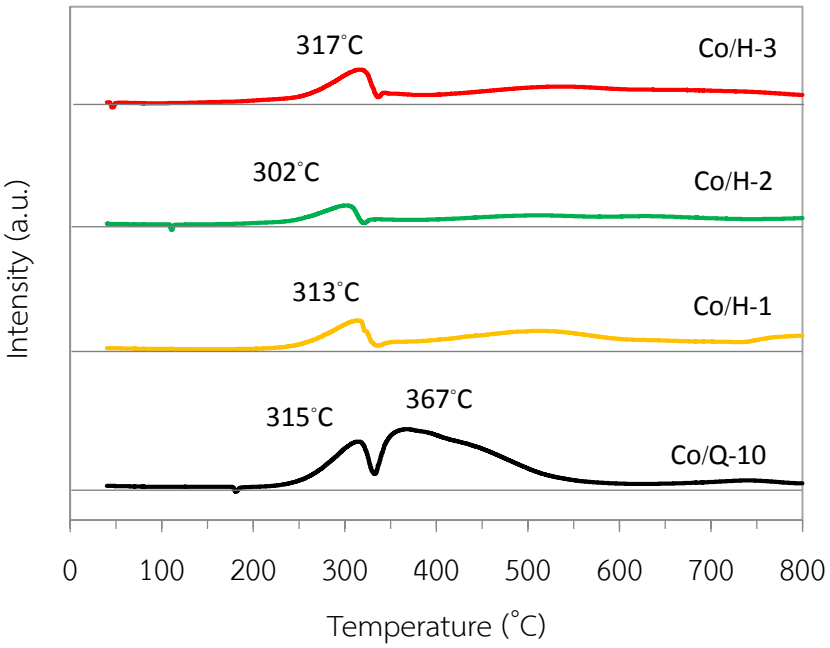

Figure 14 H_2-TPR spectra of the Co/Q-10 and Co/SHS catalysts

Table 5 Amount of hydrogen uptake in the catalysts.

Catalysts	H_2 uptake (mmol/g_{cat})[a]		Total amount (mmol/g_{cat})
	1st peak	2nd peak	
Co/Q-10	29.2	113.2	142.4
Co/H-1	19.3	81.1	100.4
Co/H-2	16.8	64.3	81.1
Co/H-3	27.1	84.6	111.7

[a]H_2 uptake evaluated by H_2-TPR

H_2-TPR profiles of cobalt based SHSs and Q-10 catalysts were shown in Figure 14. The H_2-TPR profile of Co/Q-10 shows two reduction steps. The first reduction step belongs to the reduction of Co_3O_4 to CoO phase and the second step displays CoO to Co^0 [45]. Co/Q-10 and Co/SHSs exhibit a similar reduction peak in the first range of 220-320 ° C. For the Co/Q-10 shows clearly the second peak in the range of 320-550 ° C. The first reduction step represents a sharp low-temperature peak because

the Co_3O_4 to Co phase is fast while the CoO reduction step is slow, resulting a broad profile in the second range [10]. The broad reduction peak depends on the interaction between CoO and support, which relies on CoO cluster size. The smaller CoO particles have the interaction with the support, which is stronger than larger ones. In the present study, Co_3O_4 particle size on Co/Q-10 catalyst is bigger than Co/SHS catalyst because it has larger pore sizes, leading to the second reduction peak that shows lower temperature and narrower peak. Also, the Co/Q-10 is the highest amount of hydrogen uptake at 142.4 mmol/g_{cat} (Table 5). All the three Co/SHS catalysts show the same pattern of reduction peaks. Wei et al. [43] observed the TPR profiles. When the cobalt oxide particles were located inside the CNT pores, the two reduction peaks overlapped to large extent. Therefore, the second reduction peaks of SHS catalysts are broad because Co_3O_4 particles of SHS catalysts are probably dispersed on the silica outer wall, inside the pore, and catalyst core.

The XRD patterns of the reduced Co/Q-10 and Co/H-3 at 400°C under hydrogen are presented in Figure 15, representing the characteristic peak of CoO phase and cubic Co structure overlapped at 42-44° [14, 46, 47]. The Co species in the Co/H-3 catalyst is smaller than the Co/Q-10, probably small fragments of Co_3O_4 crystallites. The Co/H-3 catalyst has a large amount of the CoO phase more than the Co/Q-10, indicating difficult to reduce for smaller Co_3O_4 particles. Moreover, this indicates the difficulties of Co_3O_4 being reduced to Co^0 because of the significant diffusion limitations in the silica shell.

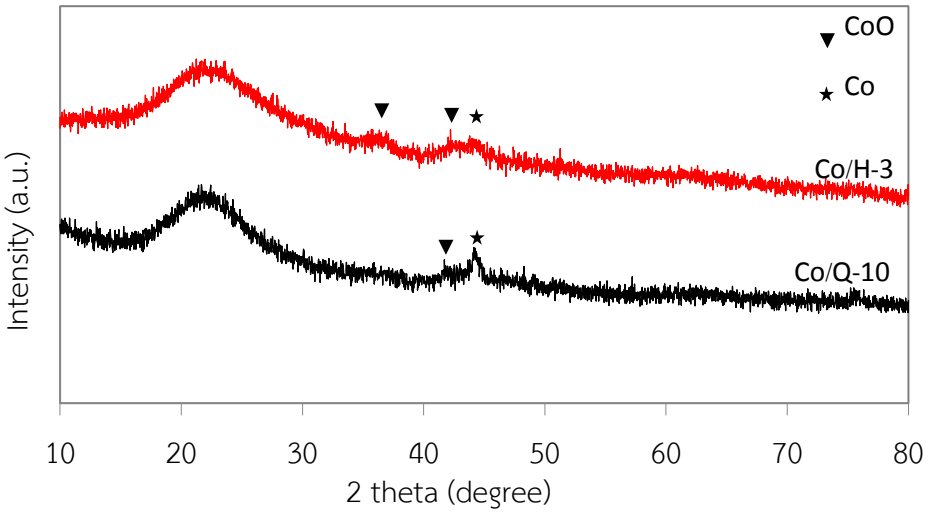

Figure 15 XRD patterns of the Co/Q-10 and Co/H-3 catalysts after reduction at 400°C.

Table 6 Summary of the chemical and textural properties of catalysts.

Catalysts	S_{BET} (m^2/g)	Pore volume (cm^3/g)[a]	Average pore size (nm)	Co_3O_4 particle size (nm)[b]	H_2 uptake ($mmol/g_{cat}$)[c]
Co/Q-10	388	1.37	14.2	13.2	141.7
Co/H-1	366	0.69	7.5	9.7	100.4
Co/H-2	392	0.59	6.0	8.8	81.1
Co/H-3	420	0.75	7.1	9.2	111.7

[a]Pore volume calculated by single point method at P/P_0 = 0.99

[b]Co_3O_4 particle size calculated by Scherrer equation

[c]H_2 uptake evaluated by H_2-TPR

4.1.2 FTS performance of the SHS catalysts

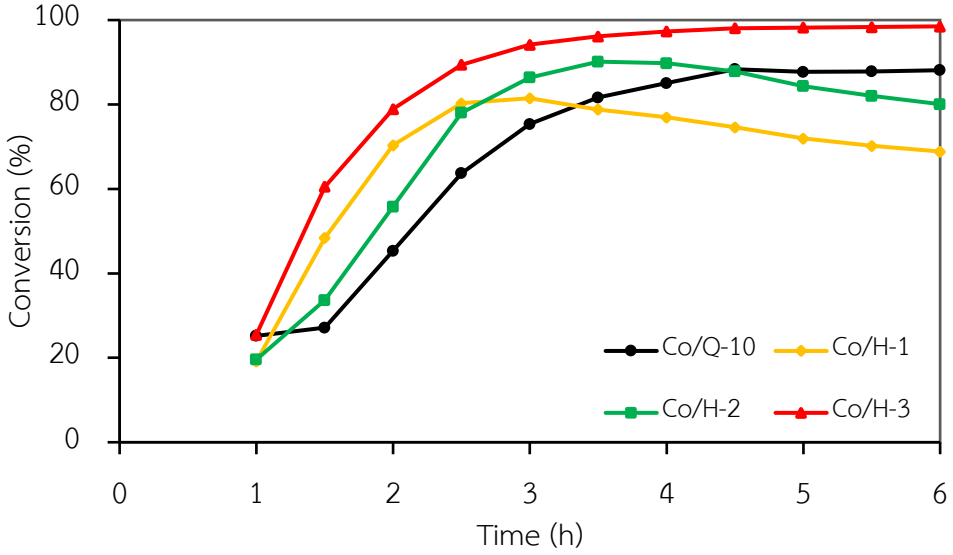

Figure 16 Catalytic performances for FTS on the Co/Q-10, Co/H-1, Co/H-2 and Co/H-3 catalysts

The reactant conversion and turn-oven frequency (TOF) are used to determine the FTS catalytic activity over all cobalt catalysts during the 6 h (Figure 16 and Table7). The best results of CO conversion were obtained for Co/H-3, which consisted of larger surface area, dispersing of small cobalt nanoparticles on the silica spheres, and small amount of micropore. The CO conversion on Co/H-3 initially increases and it is stable during 6 h, which are discovered to be 98.1% while the stability of Co/H-1 and Co/H-2 decreases significantly with an increase of the micropores due to plugging of heavy hydrocarbon inside the pores.

Table 7 The FTS performance and distribution of products from the CO and H_2.

Samples	% CO conversion	% Selectivity					C_{iso}/C_n [a]	TOF ($10^{-4}s^{-1}$)
		CO_2	CH_4	C_{2-4}	C_{5-11}	C_{12+}		
Co/Q-10	87.4	4.5	8.0	6.1	52.9	32.9	0.16	0.65
Co/H-1	72.5	8.9	10.3	10.9	51.4	27.4	0.25	0.63
Co/H-2	84.8	13.1	11.5	10.4	51.6	26.5	0.19	1.07
Co/H-3	97.4	27.5	11.9	12.3	54.8	21.0	0.14	1.03

Reaction conditions: catalyst 0.5 g, W/F = 10 ghmol $^{-1}$, H_2/CO = 2, temperature of 240 ° C, pressure of 1.0 MPa and reaction time of 6 h.

[a]iso-paraffin to n-paraffin mole ratio with chain length 4+

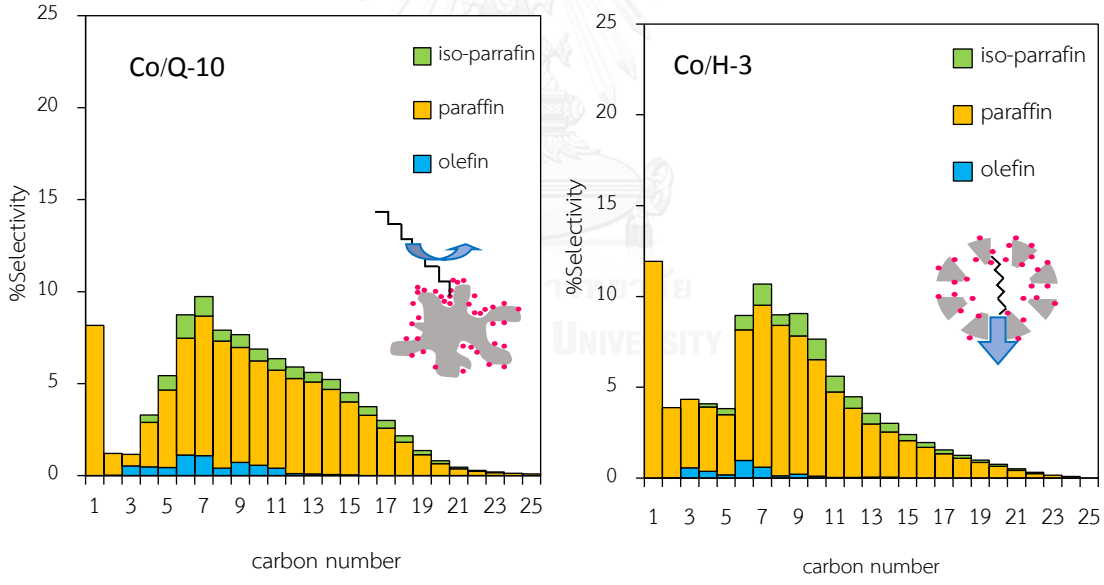

Figure 17 Product distributions over Co/Q-10 (left) and Co/H-3 (right) and the small models of the FTS reaction on the catalysts

In terms of product selectivity on the Co/H-3 and Co/Q-10, lower selectivity to the C_{12+} hydrocarbons is observed on the Co/H-3 with a value of 21.0% compared with Co/Q-10 with a value of 32.9% (Table 7). Additionally, the increased C_{2-4} and C_{5-11} selectivity on the Co/H-3 with value of 12.3% and 54.8%, respectively because CO diffusion was well-known relating to methane and hydrocarbon chain selectivity [14, 47, 48]. Additionally, the steric restrictions of the SHS catalyst for the hydrocarbon propagation results in the higher selectivity to short-chain hydrocarbons. For the paraffin distribution of the impregnated Co/Q-10 catalyst is broader than Co/H-3 catalyst with a notable tail of the distribution graph during heavier hydrocarbons. Moreover, amount of CO_2 in Co/H-3 is higher than the others (Table 7) that is caused by an increasing of the water gas shift (WGS) reaction ($CO + H_2O \leftrightarrow CO_2 + H_2$). The remaining of CoO species on the reduced Co/H-3 catalyst could be initiated the WGS [30].

4.1.3 Study of both with and without sonication during catalyst preparation.

4.1.3.1 Structural and textural of catalysts.

The influence of both with and without sonication was used during the catalyst preparation. The catalyst preparation with sonication influences physicochemical and catalytic performance because sonication is commonly used to clean or erode the solid surface [49, 50]. Also, the penetration of the active metals move inside the pore of the support. Therefore, the commercial catalyst in FTS is always prepared by impregnation method with sonication. However, the silica hollow spheres had smaller particles. If the SHS catalyst is prepared by wetness impregnation with sonication, it would be possibly induced breakage and aggregation of the silicon oxide particles due to an increased collision frequency [51].

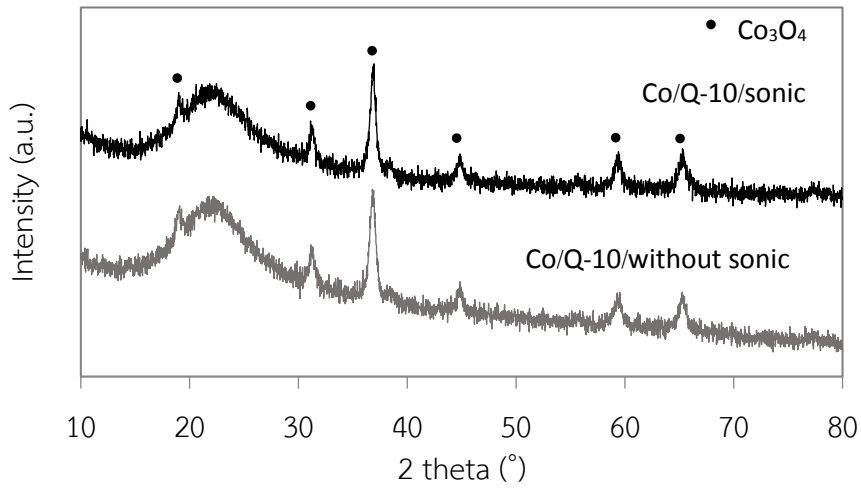

Figure 18 XRD patterns of the prepared catalysts between using and without sonication

The XRD patterns of the Co/SHS catalysts demonstrate the located peak of Co_3O_4 crystalline phase at 2θ of 19.0°, 31.3°, 36.8°, 44.7°, 59.4° and 65.2° (Figure 18). The Co_3O_4 crystallite sizes of prepared Co/Q-10 catalyst with and without sonication are calculated by Scherrer's equation, which show 13.2 and 13.7 nm, respectively (Table 8). Moreover, the observing with N_2-sorption results shows similar characteristic of prepared Co/Q-10 with and without sonication because all catalysts are prepared using the excess water in following the wet absorption method in vacuum, leading to the moving of metal precursors into the pores.

Table 8 Summary of the chemical and textural properties of catalysts.

Catalysts	S (m^2/g)			Pore volume (cm^3/g)[c]	Average pore size (nm)	Co_3O_4 particle size (nm)[d]
	Total	Micropore[a]	Mesopore[b]			
Q-10	326	31	295	1.20	14.8	-
Co/Q-10/sonic	295	29	266	1.07	14.5	13.2
Co/Q-10/without sonic	292	28	264	1.05	14.5	13.7

[a]Microporous surface area evaluated by the t-plot method.

[b]Mesoporous surface evaluated by the t-plot method.

[c]Pore volume calculated by the single point method at $P/P_0 = 0.99$

[d]Co_3O_4 particle size calculated by the Scherrer's equation.

4.1.3.2 FTS performance of the catalysts

Co/Q-10 catalysts are prepared by incipient wetness impregnation with sonication and without sonication, which give no observed change catalytic activity and product selectivity. (Table 9 and Figure 19). Bianchi et al. [52] represented the catalysts with a high amount of metal (>1 %wt), which was inessential about proving of metal dispersion on the support with sonication because %metal dispersion was analyzed by hydrogen chemisorption that indicated not different between catalyst prepared with sonication and without sonication at high amount metal e.g. 5 %wt.

Table 9 The FTS performance and distribution of products from the CO and H_2.

Samples	% CO conversion	% Selectivity					C_{iso}/C_n [a]	C_{ole}/C_n [b]
		CO_2	CH_{4+}	C_{2-4}	C_{5-11}	C_{12+}		
Co/Q-10/sonic	87.4	4.5	8.0	6.1	52.9	32.9	0.16	0.08
Co/Q-10/without sonic	87.2	7.2	8.7	5.7	50.1	35.5	0.16	0.08

Reaction conditions: catalyst 0.5 g, W/F = 10 ghmol $^{-1}$, H_2/CO = 2, temperature of 240°C, pressure of 1.0 MPa and reaction time 6 h.

[a]iso-paraffin to n-paraffin mole ratio with chain length 4+

[b]olefin to n-paraffin mole ratio with chain length 2+

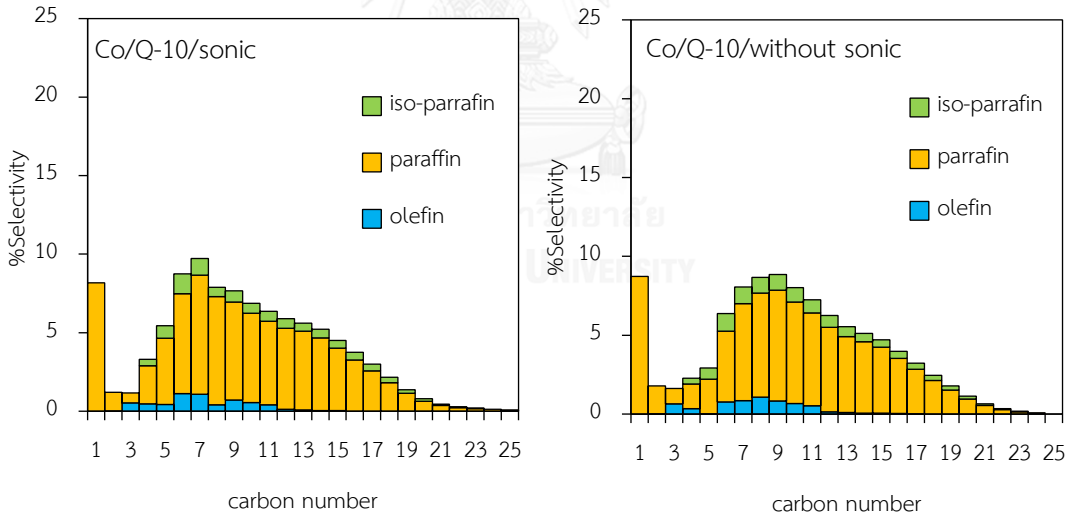

Figure 19 Product distributions over Co/Q-10 catalysts: sonication (left) and without sonication (right)

4.2 The improved catalyst with zeolite

Co/H-3 is developed by zeolite coating for increasing of the light isoparaffin selectivity because the zeolite has acid sites for improved hydrocracking and isomerization in the second step during the FTS reaction.

4.2.1 Structural and textural of catalysts.

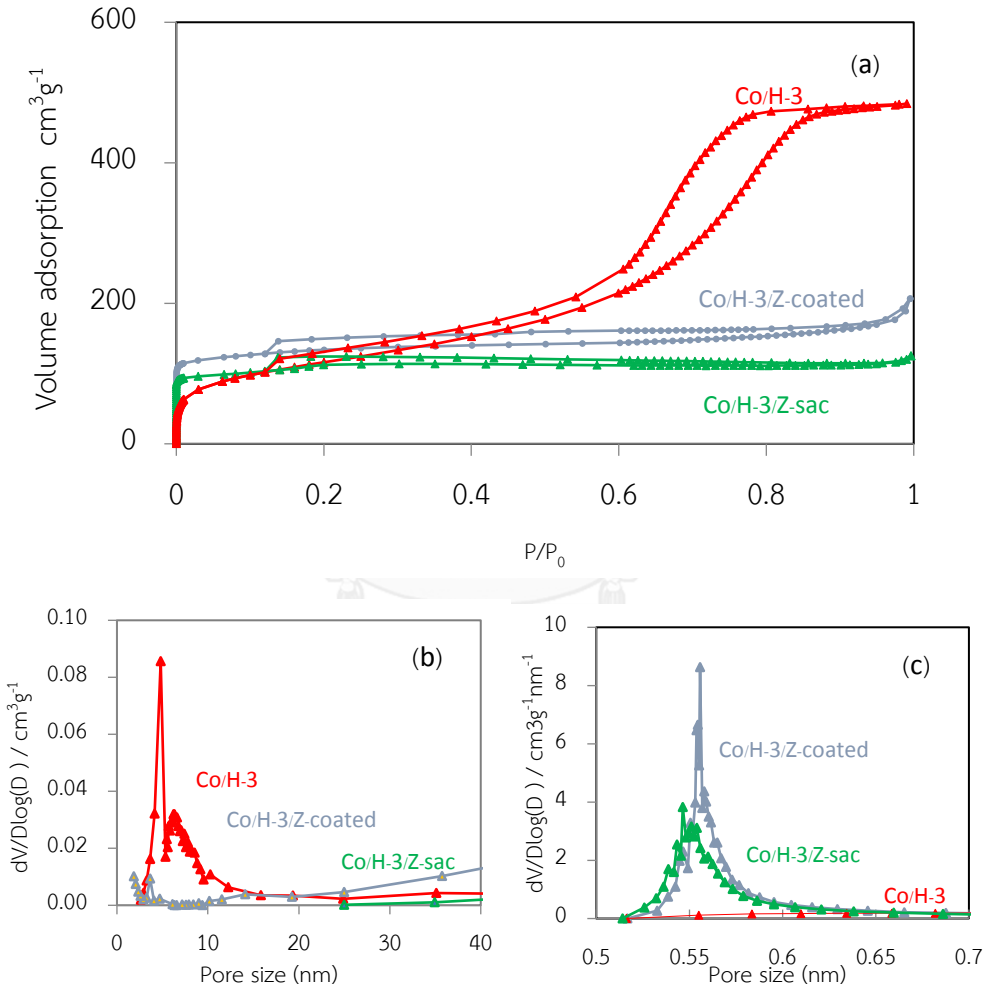

Figure 20 Nitrogen sorption isotherms of samples (a), pore size distribution of samples in mesoporous region (b) and micropore region (c)

The textual properties of zeolite coating over SHS (H-3) catalyst are prepared by hydrothermal method and SAC process, which are characterized by the N_2-sorption analysis. The N_2 adsorption–desorption isotherms and pore size distributions show in Figure 20. Specific surface area, pore size, and pore volume are summarized in Table 10. The Co/H-3 catalyst shows type-IV isotherms with H1 hysteresis loops, suggesting tubular mesopore structures. Then, the Co/H-3 catalyst is coated by ZSM-5 via hydrothermal synthesis and SAC process. Both coating methods represent type-I and type-IV isotherms which compose of micropore in catalysts. Also, the zeolite coating of both methods shows about 0.2-0.9 of relative pressure (P/P_0), containing the broad distribution of mesopores. Moreover, P/P_0 at 0.95-1.0 is observed that Co/H-3/Z catalyst was coated by hydrothermal synthesis, which has macropore more than Co/H-3/Z-SAC due to aggregation of zeolite particles. Moreover, the micropore of Co/H-3/Z coating of hydrothermal method is less than SAC process. However, mesopores in catalyst of both coating methods disappear (Figure 20 (b)) while micropores of both coating methods are more than Co/H-3 due to zeolite as microporous material. The micropores in catalyst cause to the difficult mass diffusion, leading to lower carbon monoxide conversion. Also, the zeolite coating possibly affects to destroy the silica sphere due to increased pH and the zeolite can nucleate inside the SHS, leading to decrease hollow characteristic.

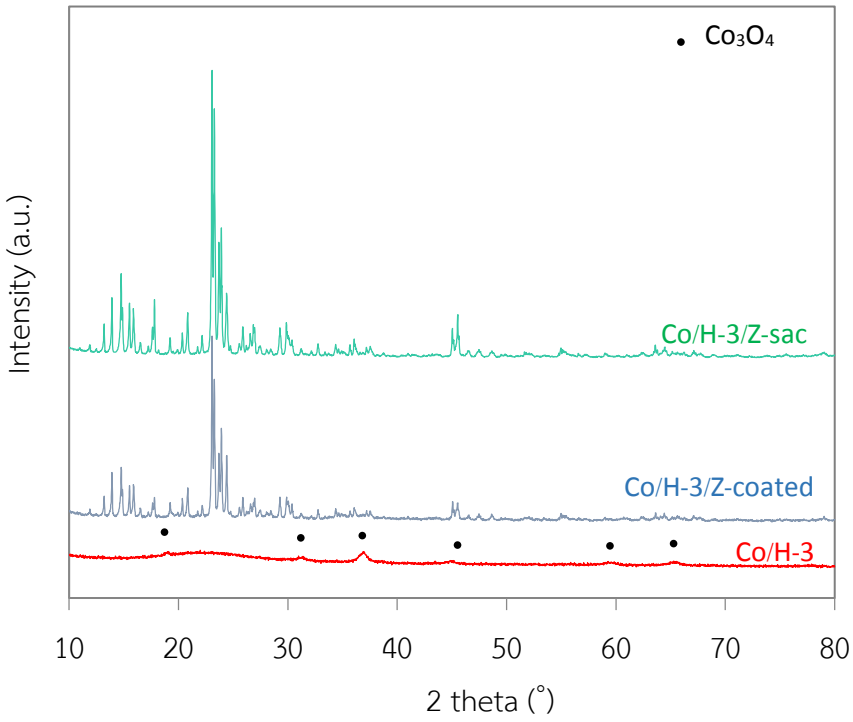

Figure 21 XRD patterns of the Co/H-3 catalyst and the coated ZSM-5 over Co/H-3 catalysts of both coated methods

The XRD patterns show the located peak of Co/H-3, Co/H-3/Z-coated, and Co/H-3/Z-sac catalysts (Figure 21). The Co_3O_4 crystallite size of the Co/H-3 is calculated from XRD patterns by the Scherrer's equation with a value of 9.2 nm. When the Co/H-3 is coated by ZSM-5, the diffraction peaks show the range of 2θ = 7-9° and 23-25°, which represent the characteristic feature of ZSM-5 structure. Nevertheless, the Co_3O_4 phases of zeolite coating disappear in XRD patterns.

Table 10 Summary of the chemical and textural properties of catalysts.

Catalysts	S (m^2/g)			Pore volume (cm^3/g)[c]	Average pore size (nm)	Co_3O_4 particle size (nm)[d]
	Total	Micropore[a]	Mesopore[b]			
Co/H-3	420	10	410	0.75	7.1	9.2
Co/H-3/Z	438	286	152	0.31	2.8	n.d.[e]
Co/H-3/Z-sac	368	163	205	0.19	2.0	n.d.

[a]Microporous surface area evaluated by the t-plot method.

[b]Mesoporous surface evaluated by the t-plot method.

[c]Pore volume calculated by the single point method at P/P_0 = 0.99

[d]Co_3O_4 particle size calculated by Scherrer equation

[e]n.d.= not determined

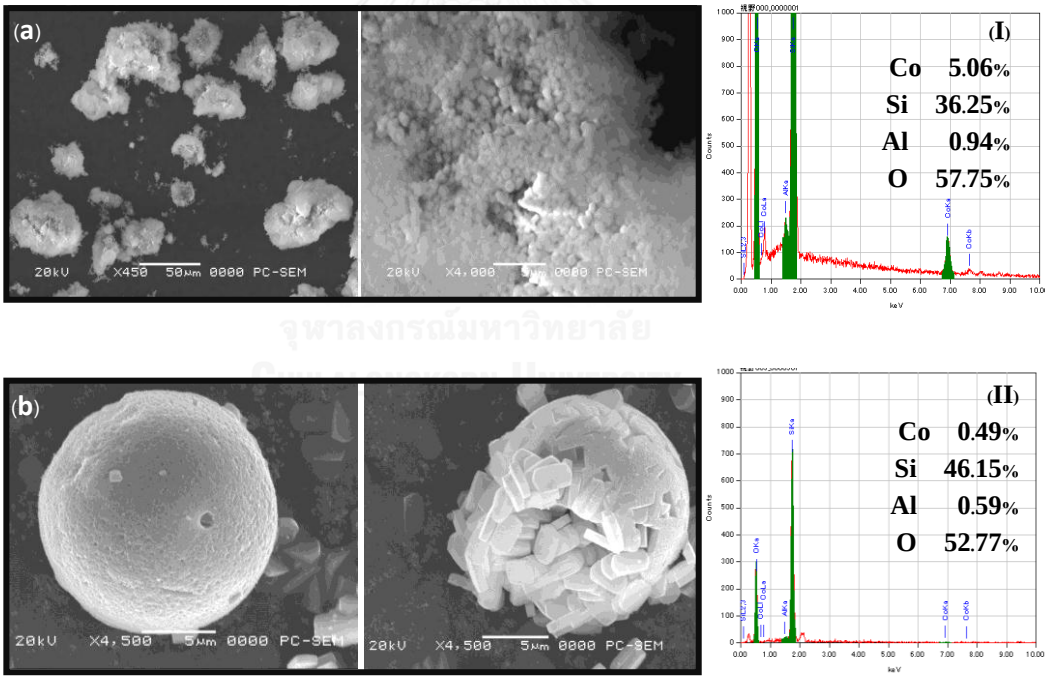

Figure 22 SEM images of samples: (a) Co/H-3/Z-coated and (b) Co/H-3/Z-SAC and EDS spectrum of (I) Co/H-3/Z-coated and (II) Co/H-3/Z-SAC catalysts

SEM images and EDS spectrums of the ZSM-5-coated Co/H-3 catalysts, synthesized with different coating methods, are presented in Figure 22. The Co/H-3/Z catalysts are observed in the SEM images that some SHS catalyst is destroyed of SAC process while sphere structure of coated catalyst by hydrothermal method disappear. Moreover, % cobalt amount of Co/H-3/Z-coated and the Co/H-3/Z-SAC are 5.06 %wt and 0.49 %wt, respectively which are analyzed by EDS. Cobalt oxide is possibly dissolved in the base solution by coated zeolite preparation.

4.2.2 FTS performance of the SHS catalysts

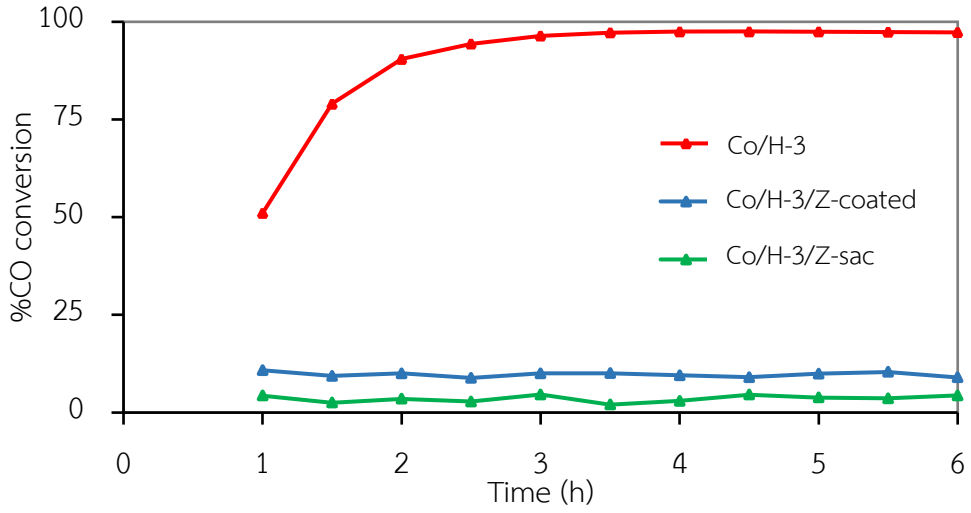

Figure 23 CO conversion of catalytic performance in FTS on the catalysts

The catalytic performance for FTS on zeolite coated cobalt catalyst compares Co/H-3 with ZSM-5-coated Co/H-3 catalysts (Figure 23). For the Co/H-3 catalyst's CO conversion is 97.4% which is the highest CO conversion. The zeolite coating exhibits a decrease in CO conversion for the hydrothermal method and SAC process at 9.6% and 3.9%, respectively. The ratio of isoparaffin to paraffin product increases to 1.27 and 1.14 of hydrothermal synthesis and SAC processes, respectively as shown in Table 11. Also, the products distribution of zeolite coating catalysts show light hydrocarbon more than Co/H-3 (Figure 24), resulting from acid sites of zeolite characteristic through

hydrocracking and isomerization [19]. However, the silicon oxide was dissolved in high pH and some zeolite particle coating around the SHS catalysts, leading to without any catalytic activity.

Table 11 The FTS performance and distribution of products from the CO and H_2.

Samples	% CO conversion	% Selectivity					C_{iso}/C_n [a]	C_{ole}/C_n [b]
		CO_2	CH_4	C_{2-4}	C_{5-11}	C_{12+}		
Co/H-3	97.4	27.5	11.9	12.3	54.8	21.0	0.14	0.04
Co/H-3/Z-coated	9.6	0	21.4	26.7	51.8	0	1.27	0.61
Co/H-3/Z-sac	3.9	0	22.0	22.8	55.2	0	1.14	1.09

Reaction conditions: catalyst 0.5 g, W/F = 10 ghmol^{-1}, H_2/CO = 2, temperature of 240 ° C, pressure of 1.0 MPa and reaction time 6 h.

[a]iso-paraffin to n-paraffin mole ratio with chain length 4+

[b]olefin to n-paraffin mole ratio with chain length 2+

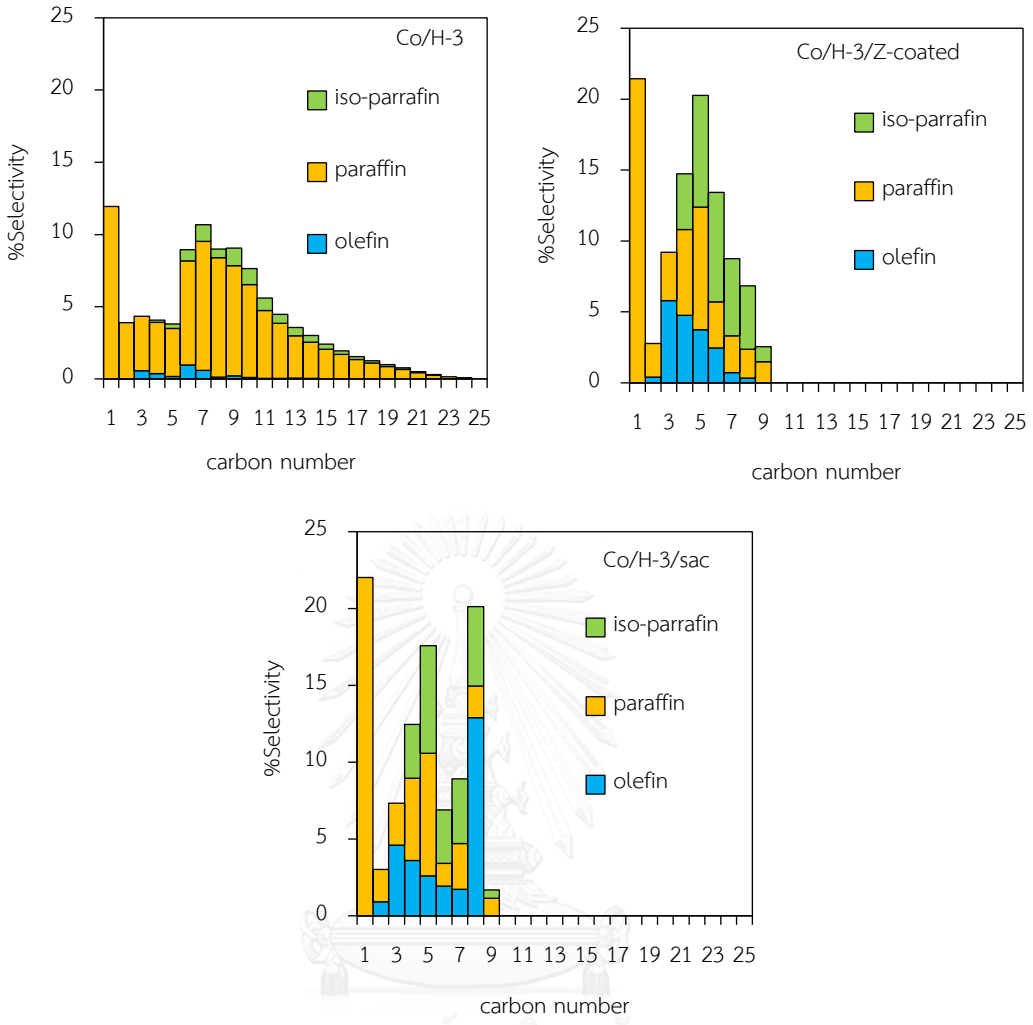

Figure 24 Product distributions over the catalysts; (a) Co/H-3, (b) Co/H-3-coated, and (c) Co/H-3-sac

CHAPTER V

CONCLUSION AND RECOMMENDATION

5.1 Conclusion

5.1.1 Preparation of the cobalt based over silica hollow sphere catalyst

The new support as SHS was successfully prepared by W/O/W multiple emulsions. The prepared SHS used sodium silicate as a silica source and NH_4HCO_3 as a silica precipitant for the mesopore generating in the SHS support. The cobalt catalysts based on SHS was impregnated by the cobalt nitrate precursor of 10%wt. The core-shell in SHS structure was confirmed by SEM images. The textural and chemical properties of the SHS catalysts compared with the commercial catalyst (Q-10) which showed the cobalt metals transfer inside the pores of support in all catalysts. The Co/H-3 showed the highest specific surface area more than 400 m^2/g and small amount of micropore. Additionally, the cobalt oxide particles size of SHS catalyst was smaller than the commercial catalyst. Moreover, the reducibility on cobalt-based SHS was the difficult reduction of Co_3O_4 to Co metal because of small cluster size and diffusion limitations of hydrogen gas in the core-shell catalyst.

5.1.2 Study of the catalytic activity of the cobalt based over silica hollow sphere catalyst in FTS

The observation in the FTS reaction with the temperature of 240°C, W/F of 10 $ghmol^{-1}$ and pressure at 1 MPa compared the SHS catalyst with commercial catalyst. The SHS as a suitable support (Co/H-3) in FTS reaction showed good catalytic activity as higher CO conversion more than 90 percent, and good selectivity with lower C_{12+} (the narrower products) because the Co/H-3 showed the high specific surface area, small cobalt cluster size, and small amount of micropore. The small amount of micropore in the catalyst assisted to decrease the plugging of heavy hydrocarbon. Moreover, the hollow sphere shape of SHS catalyst has wall of the catalyst core for

steric restriction of hydrocarbon propagation. This reason helped to decrease the catalyst deactivation, which were also an important factor in the FTS.

5.1.3 Study of the catalytic activity of the modified cobalt based over silica hollow sphere catalyst with ZSM-5 in FTS

The coated zeolite on the SHS catalyst that was ZSM-5 type was studied by two methods. There were hydrothermal synthesis and steam-assisted crystallization (SAC) process. The N_2-adsorption and desorption analysis represented much micropore in the catalysts. The XRD pattern showed the zeolite crystal of both preparation methods. And, the SEM images showed the coating of zeolite but the hydrothermal synthesis disappear the SHS shapes while the SAC process represented zeolite to cover on the SHS catalyst. The EDS spectrum exhibited the lower amount of cobalt loading on the SHS support. Thus, the problems affected to lower carbon monoxide conversion less than uncoated SHS catalyst.

5.2 Recommendation

The natural problems in FTS were wax deposition on the active phases, leading to changing activity. Therefore, the SHS support as alternative support was high surface area and there was silica wall at catalyst core which has steric restriction for controlling of chain length distribution in FTS reaction, avoiding catalyst deactivation. Moreover, it should be developed for increase selectivity and stability. For example, the SHS support was added by various amount of cobalt loading. Also, the physicochemical characteristic of located cobalt catalysts should observe the different Co species location between inner and outer surface of the SHS. Furthermore, the modification of zeolite coating should study various conditions such as pH, temperature, the time during aging and so on.

REFERENCES

1. Hu, J., F. Yu, and Y. Lu, *Application of Fischer–Tropsch Synthesis in Biomass to Liquid Conversion.* Catalysts, 2012. **2**(4): p. 303-326.
2. Wood, D.A., C. Nwaoha, and B.F. Towler, *Gas-to-liquids (GTL): A review of an industry offering several routes for monetizing natural gas.* Journal of Natural Gas Science and Engineering, 2012. **9**: p. 196-208.
3. Laan, G.P.v.d., *Kinetics, Selectivity and Scale Up of the Fischer-Tropsch Synthesis*. 1999, Groningen.
4. Zhang, Q., J. Kang, and Y. Wang, *Development of Novel Catalysts for Fischer-Tropsch Synthesis: Tuning the Product Selectivity.* ChemCatChem, 2010. **2**(9): p. 1030-1058.
5. Sheng, M., et al., *Novel catalyst structures with enhanced heat transfer characteristics.* Journal of Catalysis, 2011. **281**(2): p. 254-262.
6. Klaigaew, K., et al., *Effect of preparation methods on activation of cobalt catalyst supported on silica fiber for Fischer–Tropsch synthesis.* Chemical Engineering Journal, 2015. **278**: p. 166-173.
7. Xiong, H., et al., *Cobalt catalysts supported on a micro-coil carbon in Fischer–Tropsch synthesis: A comparison with CNTs and CNFs.* Catalysis Today, 2013. **214**: p. 50-60.
8. Chernyak, S.A., et al., *Co catalysts supported on oxidized CNTs: Evolution of structure during preparation, reduction and catalytic test in Fischer-Tropsch synthesis.* Applied Catalysis A: General, 2016. **523**: p. 221-229.
9. Xiong, H., et al., *Correlating the preparation and performance of cobalt catalysts supported on carbon nanotubes and carbon spheres in the Fischer–Tropsch synthesis.* Journal of Catalysis, 2011. **278**(1): p. 26-40.
10. Xiong, H., et al., *Fischer–Tropsch synthesis: The role of pore size for Co/SBA-15 catalysts.* Journal of Molecular Catalysis A: Chemical, 2008. **295**(1-2): p. 68-76.

11. González, O., et al., *Use of different mesostructured materials based on silica as cobalt supports for the Fischer–Tropsch synthesis.* Catalysis Today, 2009. **148**(1-2): p. 140-147.
12. Li, H., et al., *Studies on MCM-48 supported cobalt catalyst for Fischer–Tropsch synthesis.* Journal of Molecular Catalysis A: Chemical, 2006. **244**(1-2): p. 33-40.
13. Li, J., et al., *Hollow mesoporous silica sphere supported cobalt catalysts for F–T synthesis.* Catalysis Today, 2009. **148**(1-2): p. 148-152.
14. Subramanian, V., et al., *Nanoreactors: An Efficient Tool To Control the Chain-Length Distribution in Fischer–Tropsch Synthesis.* ACS Catalysis, 2016. **6**(3): p. 1785-1792.
15. Fujiwara, M., et al., *Preparation and Formation Mechanism of Silica Microcapsules (Hollow Sphere) by Water/Oil/Water Interfacial Reaction.* American Chemical Society, 2004. **16**(5420-5426).
16. Iglesia, E., *Design, synthesis, and use of cobalt-based Fischer-Tropsch synthesis catalysts.* Applied Catalysis A: General, 1997. **161**: p. 59-78.
17. Davis, B.H., *Fischer-Tropsch Synthesis: Current Mechanism and Futuristic Needs*, in *Applied Energy Research*. 2540, Kentucky: Lexington.
18. Anderson, J.R. and M. Boudart, *Catalysis Science and Technology*. 1982, New York.
19. Jahangiri, H., et al., *A review of advanced catalyst development for Fischer–Tropsch synthesis of hydrocarbons from biomass derived syn-gas.* Catal. Sci. Technol., 2014. **4**(8): p. 2210-2229.
20. Bezemer, G.L., et al., *Cobalt Particle Size Effects in the Fischer-Tropsch Reaction Studied with Carbon Nanofiber Supported Catalysts.* Journal of the American Chemical Society, 2006. **128**: p. 3956-3964.
21. Tsakoumis, N.E., et al., *Deactivation of cobalt based Fischer–Tropsch catalysts: A review.* Catalysis Today, 2010. **154**(3-4): p. 162-182.
22. Khodakov, A.Y., W. Chu, and P. Fongarland, *Advances in the Development of Novel Cobalt Fischer-Tropsch Catalysts for Synthesis of Long-Chain Hydrocarbons and Clean Fuels.* American Chemical Society, 2007. **107**(1692-1744).

23. Borg, O., et al., *Fischer–Tropsch synthesis: Cobalt particle size and support effects on intrinsic activity and product distribution.* Journal of Catalysis, 2008. **259**(2): p. 161-164.
24. Busca, G., *Preparation of Solid Catalysts.* 2014: p. 9-22.
25. Bessell, S., *Support effects in cobalt-based Fischer-Tropsch catalysis.* Applied Catalysis A: General, 1993. **96**: p. 253-268.
26. Storsater, S., et al., *Characterization of alumina-, silica-, and titania-supported cobalt Fischer–Tropsch catalysts.* Journal of Catalysis, 2005. **236**(1): p. 139-152.
27. Khodakov, A.Y., et al., *Pore-Size Control of Cobalt Dispersion and Reducibility in Mesoporous Silicas.* 2001. **105**: p. 9805-9811.
28. Khodakov, A.Y., et al., *Pore Size Effects in Fischer Tropsch Synthesis over Cobalt-Supported Mesoporous Silicas.* Journal of Catalysis, 2002. **206**(2): p. 230-241.
29. He, J., et al., *Designing a Capsule Catalyst and Its Application for Direct Synthesis of Middle Isoparaffins.* Langmuir, 2005. **21**: p. 1699-1702.
30. Xing, C., et al., *Tunable isoparaffin and olefin yields in Fischer–Tropsch synthesis achieved by a novel iron-based micro-capsule catalyst.* Catalysis Today, 2015. **251**: p. 41-46.
31. Koo, H.M., et al., *Effect of the ordered meso–macroporous structure of Co/SiO2on the enhanced activity of hydrogenation of CO to hydrocarbons.* Catal. Sci. Technol., 2016. **6**(12): p. 4221-4231.
32. Tessonnier, J.-P., et al., *Selective Deposition of Metal Nanoparticles Inside or Outside Multiwalled Carbon Nanotubes.* ACS Nano. **3**(8): p. 2081–2089.
33. Zhu, Y., et al., *Synthesis and Catalysis of Location-Specific Cobalt Nanoparticles Supported by Multiwall Carbon Nanotubes for Fischer–Tropsch Synthesis.* Langmuir, 2012. **28**(21): p. 8275-8280.
34. Rytter, E., N.E. Tsakoumis, and A. Holmen, *On the selectivity to higher hydrocarbons in Co-based Fischer–Tropsch synthesis.* Catalysis Today, 2016. **261**: p. 3-16.
35. Yang, J., et al., *Fischer–Tropsch Synthesis on Co-based Catalysts in a Microchannel Reactor. Effect of Temperature and Pressure on Selectivity and*

Stability. Catalysts and Catalysis: Advances and Applications, 2003. **223**: p. 259-266.

36. Choudhury, H.A. and V.S. Moholkar, *An Optimization Study of Fischer–Tropsch Synthesis Using Commercial Cobalt Catalyst.* International Journal of Scientific Engineering and Technology, 2013. **2**(1): p. 31-39.
37. Deugd, R.M.d., F. Kapteijn, and J.A. Moulijn, *Trends in Fischer–Tropsch reactor technology—opportunities for structured reactors.* Topics in Catalysis, 2003. **26**: p. 1-4.
38. Guettel, R. and T. Turek, *Comparison of different reactor types for low temperature Fischer–Tropsch synthesis: A simulation study.* Chemical Engineering Science, 2009. **64**(5): p. 955-964.
39. Wang, T., J. Wang, and Y. Jin, *Slurry Reactors for Gas-to-Liquid Processes: A Review.* Ind. Eng. Chem, 2007. **46**.
40. EIGENBERGER, G. and W. RUPPEL, *Catalytic Fixed-Bed Reactors*. 2015, Stuttgart: Germany.
41. Xing, C., et al., *Tunable isoparaffin and olefin synthesis in Fischer–Tropsch synthesis achieved by composite catalyst.* Fuel Processing Technology, 2015. **136**: p. 68-72.
42. Xie, W., et al., *Effect of catalyst confinement and pore size on Fischer-Tropsch synthesis over cobalt supported on carbon nanotubes.* Science China Chemistry, 2012. **55**(9): p. 1811-1818.
43. Chen, W., et al., *Effect of Confinement in Carbon Nanotubes on the Activity of Fischer-Tropsch Iron Catalyst.* Journal of the American Chemical Society, 2008. **130**: p. 9414–9419.
44. Cheng, K., et al., *Pore size effects in high-temperature Fischer–Tropsch synthesis over supported iron catalysts.* Journal of Catalysis, 2015. **328**: p. 139-150.
45. Witoon, T., M. Chareonpanich, and J. Limtrakul, *Effect of hierarchical meso-macroporous silica supports on Fischer-Tropsch synthesis using cobalt catalyst.* Fuel Processing Technology, 2011. **92**(8): p. 1498-1505.

46. Ernst, B., et al., *Study on a cobalt silica catalyst during reduction and Fischer-Tropsch reaction: In situ EXAFS compared to XPS and XRD* Catalysis Today, 1998. **39**: p. 329-341.

47. Shi, L., et al., *Surface Impregnation Combustion Method to Prepare Nanostructured Metallic Catalysts without Further Reduction: As-Burnt Co/SiO2Catalysts for Fischer–Tropsch Synthesis.* ACS Catalysis, 2011. **1**(10): p. 1225-1233.

48. Prieto, G., et al., *Cobalt supported on morphologically tailored SBA-15 mesostructures: The impact of pore length on metal dispersion and catalytic activity in the Fischer–Tropsch synthesis.* Applied Catalysis A: General, 2009. **367**(1-2): p. 146-156.

49. Bianchi, C.L., et al., *Preparation of Pd/C catalysts via ultrasound: a study of the metal distribution.* Ultrasonics Sonochemistry, 1997. **4**: p. 317 320.

50. Kumar, N., et al., *Synthesis of Pt modified ZSM-5 and beta zeolite catalysts: influence of ultrasonic irradiation and preparation methods on physico-chemical and catalytic properties in pentane isomerization.* Ultrason Sonochem, 2007. **14**(2): p. 122-30.

51. Hashem, M.M., et al., *Increasing the Reactivity of Silica Fume Particles Using Indirect Sonication: Effect of Process Parameters.* International Journal of Modern Trends in Engineering and Research, 2015. **2**(7): p. 2393-8161.

52. Bianchi, C.L., et al., *Influence of ultrasound on the preparation of ruthenium catalysts supported on alumina.* Ultrasonics Sonochemistry, 1994. **1**(1): p. S47-S49.

APPENDIX

APENDIX

1. Calculation

1.1 Calculation for preparation of cobalt loading, 10%wt on supports

10%wt Co/SiO_2 catalyst was prepared by wetness impregnation method

Using the cobalt nitrate hexahydrate ($Co(NO_3)_2{\cdot}6H_2O$) as a precursor

Co (MW = 58.93 g/mol)

$Co(NO_3)_2{\cdot}6H_2O$ (MW = 291.31 g/mol)

10%wt Co/SiO_2: SiO_2 = 90 g and Co = 10 g

If the support was weighted 5 g, Co = $\frac{10\times5}{90}$ = 0.5556 g

Co 58.93 g from $Co(NO_3)_2{\cdot}6H_2O$ 291.31 g

Therefore, Co 0.5556 g, weight $Co(NO_3)_2{\cdot}6H_2O$ $\frac{291.31\times0.5556}{58.93}$ = 2.7463g

Amount of water

Volume of support about 1 ml/g

Using support = 5 g, Volume of water = 5×1 = 5 ml

1.2 Calculation for preparation of coated zeolite over the SHS catalyst

1.2.1 Hydrothermal synthesis

Molar ratio of TEOS/TPAOH/H_2O/EtOH/$Al(NO_3)_3$ = 1:0.25:60:4:0.0125

Chemicals	MW (g/mol)	Density (g/cm^3)
Silica (SiO_2)	60.09	2.20
TEOS	208.33	0.93
10% TPAOH	203.36	1.00
H_2O	18.00	1.00
EtOH, 99.5%	46.07	0.79
$Al(NO_3)_3{\cdot}H_2O$, 99.5%	264.10	1.72

Starting of TEOS = 0.0161 mol

1 TEOS:	0.25 TPAOH:	60 H_2O:	4 EtOH:	0.00125 $Al(NO_3)_3$	
1(0.0161)	0.25(0.0161)	60(0.0161)	4(0.0161)	0.00125(0.0161)	
0.0161	0.00402	0.966	0.0644	0.0000201	mol

Therefore, the chemicals were weight by,

TEOS = 0.0161×208.33 = 3.6 g

TPAOH = $\frac{100 \times 0.00402 \times 203.36}{10}$ = 8.2 g

H_2O = 0.966×18 = 17.4 g

EtOH = $\frac{100 \times 0.0644 \times 46.07}{99.5}$ = 3.0 g

$Al(NO_3)_3 = \frac{100 \times 0.0000201 \times 264.1}{99.5}$ = 0.0053g

1.2.2 SAC process

The micro-capsule catalyst with Co/H-3 core and H-ZSM-5 zeolite shell was prepared by using via SAC process

Chemicals	MW (g/mol)	Density (g/cm^3)	Used (g)
Co/H-3 catalyst	-	-	1.00
TEOS	208.33	0.93	3.26
10% TPAOH	203.36	1.00	3.03
H_2O	18.00	1.00	10.72
Al(i-propoxide), ≥98%	204.25	1.035	0.026

Calculation to molar ratio

a TEOS:	b TPAOH:	c H_2O:	d Al(i-propoxide)	
$\frac{3.26}{208.33}$	$\frac{3.03\times10}{100\times203.36}$	$\frac{10.72}{18.00}$	$\frac{0.026}{204.25}$	
0.016	0.0015	0.60	0.000125	mol
1	0.01	38	0.008	mol

Therefore, molar ratio of Al_2O_3:SiO_2:H_2O: TPAOH of 0.008: 1: 38: 0.01

2. Turn over frequency (TOF)

$$TOF = \frac{\left(\frac{mol\ converted\ substrate \times \%conversion}{mol\ of\ catalyst} \right)}{time}$$

- Mol converted substrate (CO conversion, mol/g_{cat}h)

$$= \frac{\frac{PV}{RT} \times \%COgas \times \%COconv}{g_{cat}}$$

- Mol of Co catalysts

From $Co_3O_4 + 4H_2 \rightarrow 3Co + 4H_2O$

$$= \frac{H_2 uptake(mol/g_{cat}) \times 3}{4}$$

- Time = 1 h =3600 s

Example of the Co/Q-10

$$TOF = \frac{\frac{0.0284 mol\,g^{-1} \times 0.874}{0.1068 mol\,g^{-1}}}{3600 s}$$

Therefore,

TOF of Q-10 = 0.65 ($10^{-4}s^{-1}$)

TOF of H-1 = 0.63 ($10^{-4}s^{-1}$)

TOF of H-2 = 1.07 ($10^{-4}s^{-1}$)

TOF of H-3 = 1.03 ($10^{-4}s^{-1}$)

3. Calculation of CO conversion and hydrocarbon product selectivity

Reaction conditions: catalyst 0.5 g, W/F = 10 ghmol^{-1}, H_2/CO = 2, temperature of 240$^{\circ}C$, pressure of 1.0 MPa and reaction time 6 h.

$$\%CO\,conversion = \frac{\left(\frac{CO}{Ar}\right)_{inlet} - \left(\frac{CO}{Ar}\right)_{outlet}}{\left(\frac{CO}{Ar}\right)_{inlet}} \times 100$$

$$CO_2\ selectivity\,(\%) = \frac{moles\ of\ CO_2\ produced}{moles\ of\ CO\ conversion} \times 100$$

$$CH_4\ selectivity\,(\%) = \frac{moles\ of\ CH_4\ produced}{moles\ of\ CO\ conversion - moles\ of\ CO_2\ produced} \times 100$$

$$C_{12+}\ selectivity\,(\%) = 100 - (CH_4\ selectivity) - (C_{2-11}\ selectivity)$$

$$C_{iso}\,/\,C_n = \frac{moles\ of\ isoparaffin\ in\ produced}{moles\ of\ paraffin\ in\ produced} \times 100$$

$$C_{ole}\,/\,C_n = \frac{moles\ of\ olefin\ in\ produced}{moles\ of\ paraffin\ in\ produced} \times 100$$

For example,

Effluent gas composition

Time on stream (h)		1	2	3	4	5	6
Area	Ar	16847	22515	43785	64486	77484	80836
	CO	136810	133579	117032	104607	103159	104081
	CH_4	2338	6010	21042	34835	42759	45941
	CO_2	0	3840	18652	31655	37499	38750

Syngas

Syngas	Composition (%)	TCD(Area)
Ar	4.1	13014
CO	32.5	141276
(CO/Ar)	7.93	10.86

Standard gas

Standard gas	Composition (%)	TCD (Area)	FID (Area)
CO	5.03	23320	
CH4	4.96	18953.67	585436
CO2	5.12	22478.33	

Time at 6 h

$$\%CO\,conversion = \frac{\left(\frac{141276}{13014}\right)_{inlet} - \left(\frac{104081}{80836}\right)_{outlet}}{\left(\frac{141276}{13014}\right)_{inlet}} \times 100 = 88.1\%$$

$$CO_2\ selectivity\,(\%) = \frac{0.001281}{0.02864} \times 100 = 4.47\%$$

$$CH_4\ selectivity\,(\%) = \frac{0.001745}{0.02864 - 0.001281} \times 100 = 6.38\%$$

$$C_2\ selectivity\,(\%) = 1.1820 + 0.01769 + 0 = 1.20\%$$

$$C_3\ selectivity\,(\%) = 0.6283 + 0.5270 + 0 = 1.15\%$$

$$C_4\ selectivity\,(\%) = 2.4221 + 0.4793 + 0.3943 = 3.30\%$$

$$C_5\ selectivity\,(\%) = 4.2159 + 0.4315 + 0.7887 = 5.44\%$$

.

.. $C_{11}\ selectivity\,(\%) = 5.3276 + 0.3993 + 0.6258 = 6.35\%$

$$\therefore\ C_{12+}\ selectivity\,(\%) = 100 - (6.38 + 1.20 + 1.15 + 3.30 + 5.44 + ... + 6.35) = 33.5\%$$

Determination of CO conversion and gas product selectivity

Details: Co/Q-10, Flow rate = 19.8 ml/min, T = 240 ° C, P = 1 MPa, W/F = 10 ghmol^{-1}, catalyst weight 0.507 g

Time (h)		1	2	3	4	5	6
Area	Ar	16847	22515	43785	64486	77484	80836
	CO	136810	133579	117032	104607	103159	104081
	CH_4	2338	6010	21042	34835	42759	45941
	CO_2	0	3840	18652	31655	37499	38750
CO conversion (%)		25.2	45.3	75.4	85.1	87.7	88.1
Flowrate (s/10ml)		210.587	204.807	217.767	175.927	206.767	208.780
Gas produced (mol/h)		0.007	0.008	0.007	0.009	0.007	0.007
CH_4 produced		0.006	0.016	0.055	0.091	0.112	0.120
CO_2 produced		0.000	0.009	0.042	0.072	0.085	0.088
CH_4C-mol (mol/g·h)		0.000	0.000	0.001	0.002	0.002	0.002
CO_2C-mol (mol/g·h)		0.000	0.000	0.001	0.001	0.001	0.001
CO (mol/g·h)		0.008	0.015	0.024	0.028	0.029	0.029
CH_4 sel (mol%)		1.075	1.593	3.205	5.948	6.015	6.377
CO_2 sel (mol%)		0.000	0.878	2.413	4.493	4.390	4.472
C_{2+} sel (mol%)		98.925	98.393	96.716	93.773	93.708	93.325

Determination of CO conversion and gas product selectivity

Details: Co/H-1, Flow rate = 19.68 ml/min, T = 240 ° C, P = 1 MPa, W/F = 10 ghmol^{-1}, catalyst weight 0.504 g

Time (h)		1	2	3	4	5	6
Area	Ar	15469	33357	46467	42723	38346	35827
	CO	135806	107319	93417	106883	116789	121152
	CH_4	906	13041	21147	19474	17181	15943
	CO_2		23355	38094	30177	22244	18100
CO conversion (%)		19.1	70.4	81.5	77.0	71.9	68.8
Flowrate (s/10ml)		62.793	49.220	60.947	60.133	54.053	52.287
Gas produced (mol/h)		0.024	0.031	0.025	0.026	0.028	0.029
CH_4 produced		0.013	0.026	0.027	0.032	0.027	0.025
CO_2 produced		0.015	0.027	0.025	0.031	0.025	0.021
CH_4C-mol (mol/g·h)		0.001	0.002	0.001	0.002	0.002	0.001
CO_2C-mol (mol/g·h)		0.001	0.002	0.001	0.002	0.001	0.001
CO (mol/g·h)		0.013	0.019	0.018	0.019	0.018	0.017
CH_4 sel (mol%)		4.994	9.349	8.169	9.140	9.413	9.276
CO_2 sel (mol%)		5.483	9.031	6.995	8.133	7.947	7.230
C_{2+} sel (mol%)		94.716	89.723	91.216	90.050	89.775	90.001

Determination of CO conversion and gas product selectivity

Details: Co/H-2, Flow rate = 19.72 ml/min, T = 240 ° C, P = 1 MPa, W/F = 10 ghmol^{-1}, catalyst weight 0.505 g

Time (h)		1	2	3	4	5	6
Area	Ar	15815	25360	49570	58674	51543	46348
	CO	138072	121652	73212	65264	87565	100301
	CH_4	759	8641	28933	35098	29867	25565
	CO_2		12911	53788	65004	48528	36281
CO conversion (%)		19.6	55.8	86.4	89.8	84.3	80.1
Flowrate (s/10ml)		178.650	152.427	118.687	103.180	93.253	86.960
Gas produced (mol/h)		0.009	0.010	0.013	0.015	0.016	0.018
CH_4 produced		0.002	0.023	0.076	0.092	0.078	0.067
CO_2 produced		0.000	0.029	0.123	0.148	0.111	0.083
CH_4C-mol (mol/g·h)		0.000	0.000	0.002	0.003	0.003	0.002
CO_2C-mol (mol/g·h)		0.000	0.001	0.003	0.004	0.004	0.003
CO (mol/g·h)		0.006	0.018	0.028	0.029	0.027	0.026
CH_4 sel (mol%)		0.532	2.572	7.783	10.918	10.710	10.119
CO_2 sel (mol%)		0.000	3.236	11.185	14.967	13.154	11.111
C_{2+} sel (mol%)		99.468	97.342	91.237	87.160	87.667	88.616

Determination of CO conversion and gas product selectivity

Details: Co/H-3, Flow rate = 19.49 ml/min, T = 240 ° C, P = 1 MPa, W/F = 10 ghmol^{-1}, catalyst weight 0.499 g

Time (h)		1	2	3	4	5	6
Area	Ar	21768	35938	39456	40470	40143	39788
	CO	115714	37180	15422	10937	11027	11619
	CH_4	17137	59852	66704	6578	63998	62426
	CO_2	17169	84610	107438	114017	115122	114343
CO conversion (%)		51.0	90.5	96.4	97.5	97.5	97.3
Flowrate (s/10ml)		96.453	90.880	96.653	92.207	86.787	89.167
Gas produced (mol/h)		0.016	0.017	0.016	0.017	0.018	0.017
CH_4 produced		0.045	0.157	0.175	0.017	0.167	0.163
CO_2 produced		0.039	0.193	0.245	0.260	0.262	0.260
CH_4C-mol (mol/g·h)		0.001	0.005	0.006	0.001	0.006	0.006
CO_2C-mol (mol/g·h)		0.001	0.007	0.008	0.009	0.009	0.009
CO (mol/g·h)		0.017	0.029	0.031	0.032	0.032	0.032
CH_4 sel (mol%)		9.334	23.199	23.628	2.497	26.555	24.924
CO_2 sel (mol%)		7.527	22.206	24.882	27.364	29.367	28.436
C_{2+} sel (mol%)		89.906	70.179	68.546	96.562	62.405	65.173

Determination of CO conversion and gas product selectivity

Details: Co/Q-10 without sonication, Flow rate = 19.72 ml/min, T = 240 °C, P = 1 MPa, W/F = 10 ghmol^{-1}, catalyst weight 0.505 g

Time (h)		1	2	3	4	5	6
Area	Ar	20690	26477	46611	62196	72614	74902
	CO	134708	118946	93909	92409	99592	106918
	CH_4	5114	21154	44524	48566	47236	45657
	CO_2	6021	16771	40402	47838	47632	44870
CO conversion (%)		40.0	58.6	81.4	86.3	87.4	86.9
Flowrate (s/10ml)		207.180	180.747	175.667	159.607	159.747	160.300
Gas produced (mol/h)		0.007	0.009	0.009	0.010	0.010	0.010
CH_4 produced		0.013	0.055	0.117	0.127	0.124	0.119
CO_2 produced		0.014	0.038	0.092	0.109	0.108	0.102
CH_4C-mol (mol/g·h)		0.000	0.001	0.002	0.002	0.002	0.002
CO_2C-mol (mol/g·h)		0.000	0.001	0.002	0.002	0.002	0.002
CO (mol/g·h)		0.013	0.019	0.026	0.028	0.028	0.028
CH_4 sel (mol%)		1.535	5.062	8.112	9.327	8.942	8.626
CO_2 sel (mol%)		1.548	3.375	6.021	7.404	7.277	6.872
C_{2+} sel (mol%)		98.441	94.761	91.368	89.928	90.356	90.737

Determination of CO conversion and gas product selectivity

Details: Co/H-3/Z-coated, Flow rate = 19.72 ml/min, T = 240°C, P = 1 MPa, W/F = 10 ghmol^{-1}, catalyst weight 0.505 g

Time (h)		1	2	3	4	5	6
Area	Ar	14065	14052	14052	14059	14118	14011
	CO	136141	137246	137246	138056	138040	138405
	CH_4	1857	2015	2015	1886	1837	1804
	CO_2						
CO conversion (%)		10.8	10.0	10.0	9.5	9.9	9.0
Flowrate (s/10ml)		32.220	32.047	31.033	27.327	30.713	28.113
Gas produced (mol/h)		0.048	0.048	0.050	0.056	0.050	0.055
CH_4 produced		0.005	0.005	0.005	0.005	0.005	0.005
CO_2 produced		0.000	0.000	0.000	0.000	0.000	0.000
CH_4C-mol (mol/g·h)		0.000	0.001	0.001	0.001	0.000	0.001
CO_2C-mol (mol/g·h)		0.000	0.000	0.000	0.000	0.000	0.000
CO (mol/g·h)		0.004	0.003	0.003	0.003	0.003	0.003
CH_4 sel (mol%)		13.033	15.363	15.864	17.722	14.757	17.464
CO_2 sel (mol%)		0.000	0.000	0.000	0.000	0.000	0.000
C_{2+} sel (mol%)		86.967	84.637	84.136	82.278	85.243	82.536

Determination of CO conversion and gas product selectivity

Details: Co/H-3/Z-sac, Flow rate = 19.60 ml/min, T = 240 °C, P = 1 MPa, W/F = 10 ghmol^{-1}, catalyst weight 0.502 g

Time (h)		1	2	3	4	5	6
Area	Ar	13322	13205	13368	13138	13235	13280
	CO	138352	138325	138395	138386	138130	137856
	CH_4	860	894	871	863	861	856
	CO_2						
CO conversion (%)		4.3	3.5	4.6	3.0	3.9	4.4
Flowrate (s/10ml)		29.020	28.193	28.233	28.553	27.927	28.760
Gas produced (mol/h)		0.053	0.054	0.054	0.054	0.055	0.053
CH_4 produced		0.002	0.002	0.002	0.002	0.002	0.002
CO_2 produced		0.000	0.000	0.000	0.000	0.000	0.000
CH_4C-mol (mol/g·h)		0.000	0.000	0.000	0.000	0.000	0.000
CO_2C-mol (mol/g·h)		0.000	0.000	0.000	0.000	0.000	0.000
CO (mol/g·h)		0.001	0.001	0.002	0.001	0.001	0.001
CH_4 sel (mol%)		16.862	22.312	16.418	25.100	19.700	16.774
CO_2 sel (mol%)		0.000	0.000	0.000	0.000	0.000	0.000
C_{2+} sel (mol%)		83.138	77.688	83.582	74.900	80.300	83.226

VITA

Miss Thachapan Atchimarungsri was born on February 11, 1992 in Bangkok, Thailand. She graduated with Bachelor's degree of science, majoring in Chemistry, Faculty of Science, Thammasat University in 2014. She has continued her study in Master's degree, majoring in Petrochemistry and Polymer Science, Faculty of Science, Chulalongkorn University, Bangkok, Thailand since 20014 and finished her study in 2016.

Presentation Experience

Poster presentation: FISCHER- TROPSCH SYNTHESIS OVER COBALT SUPPORTED ON SILICA HOLLOW SPHERE CATALYST. The 5th Asian Conference on Innovative Energy and Environmental Chemical Engineering (ASCON-IEEChE),13-16/11/2016, Yokohama, Japan